

Coherent third-order spectroscopic probes of molecular chirality

Darius Abramavicius and Shaul Mukamel

Chemistry Department, University of California, Irvine, California 92697-2025

(Received 9 December 2004; accepted 19 January 2005; published online 5 April 2005)

The third-order optical response of a system of coupled localized anharmonic vibrations is studied using a Green's function solution of the nonlinear exciton equations for bosonized excitons, which are treated as interacting quasiparticles. The explicit calculation of two-exciton states is avoided and the scattering of quasiparticles provides the mechanism of optical nonlinearities. To first-order in the optical wave vector we find several rotationally invariant tensor components for isotropic ensembles which are induced by chirality. The nonlocal nonlinear susceptibility tensor is calculated for infinitely large periodic structures in momentum space, where the problem size reduces to the exciton interaction radius. Applications are made to α and 3_{10} helical infinite peptides. © 2005 American Institute of Physics. [DOI: 10.1063/1.1869495]

I. INTRODUCTION

Laser pulses are characterized both by their carrier frequencies ω and wave vectors \mathbf{k} . The optical response of typical molecules, which are smaller than the wavelength of light, can be calculated in the dipole approximation where the wave vector only provides an overall phase for the electric field and can be set to zero. The relevant molecular information is then extracted from the frequency spectrum (or time dependence) through the eigenstates and transition dipole matrix. Structural information enters only indirectly via the dependence of couplings and frequencies on the geometry.

The wave vector does play an important role in the spectroscopy of extended chiral systems (these are “handed” systems which are distinct from their mirror images^{1,2}), where the phase of the electric field does vary across the molecule. For this reason certain tensor components of the response function, which vanish in the dipole approximation, become finite to first order in the wave vector. A common example for such chirally-sensitive, wave vector-induced, effects is circular dichroism (CD)—the difference absorption of left- and right-handed circularly polarized light which is related to the rotation of polarization vector of the propagating optical field—phenomenon known as optical activity (OA).^{1,3-5}

Due to its high sensitivity to microscopic structure, CD spectroscopy of electronic transitions of proteins (ECD) in the visible and UV has become an important tool for structure determination.⁵⁻⁸ ECD of proteins in the 180–260 nm range shows mainly two transitions: 190 nm ($\pi-\pi^*$) and 220 nm ($n-\pi^*$).⁶⁻¹¹ Based on the relative amplitudes of different transitions in the CD spectrum proteins have been classified as α -rich, β -rich, and P_2 structures. A well-developed theoretical framework relates the CD spectrum to peptide structure. The matrix method^{12,13} is based on a set of parameters describing each chromophoric group in the protein: the parameters represent the charge distributions of all relevant ground and excited electronic states, the electric and magnetic transition densities between different states, and the coordinates of each chromophoric group, coupled by electro-

static interactions. The peptide group parameters are usually computed by semiempirical techniques.^{10,14-16}

The infrared OA of proteins shows intense peaks and high sensitivity to peptide backbone. Vibrational circular dichroism (VCD) (Refs. 17–19) and Raman optical activity (ROA), which involves differential inelastic scattering of the circularly polarized visible radiation,^{1,20-22} have focused mostly on the amide I, CO stretch, (1600–1700 cm^{-1}) and amide II, CN stretch, (1500–1600 cm^{-1}) transitions; the ROA has also routinely provided protein spectra down to $\sim 700 \text{ cm}^{-1}$.²³⁻²⁷ The CD spectrum of α -helical peptides in the amide I band shows a distinct sigmoidally shaped band at 1658 cm^{-1} that has its negative lobe blue shifted with respect to its positive lobe; the 1550 cm^{-1} amide II band shows a negative VCD band that overlaps with a larger negative band at 1520 cm^{-1} .²⁶ The other CH and NH stretching modes (3000–3300 cm^{-1}) give a very strong VCD signal at 3300 cm^{-1} with a distorted sigmoidal shape.²⁴ 3_{10} helices show similar spectra.^{23,24,26} Recent studies of α -helix, 3_{10} -helix, β -sheet, and poly(Pro)II helix reveal characteristic VCD bandshapes.²⁵ β -sheet has weak negative amide I VCD band, while poly(Pro)II resembles an inverted α -helix. VCD of β -sheet hairpins is similar to β -sheets.^{27,28} Advances in *ab initio* calculations of vibrational electric and magnetic transition dipoles and their interferences lead to highly accurate determination of vibrational absorption and VCD for small molecules.²⁹⁻³² These allow the transfer of property tensors from smaller to larger systems of coupled vibrations.³³ The VCD of dipeptides in the amide I region was calculated recently and a map of VCD amplitudes as a function of dihedral angles was created³⁴ which showed very good agreement with experiment for a tripeptide.¹⁹

Pattern recognition and decomposition algorithms for protein structure determination allow to distinguish between α -helical and β -sheet formations using ECD (Refs. 7, 35, and 36), VCD (Ref. 37), and ROA (Refs. 38 and 39). Different regions associated with particular structures were identified and reflect geometrical changes (peptide folding) as a function of external perturbations.²²

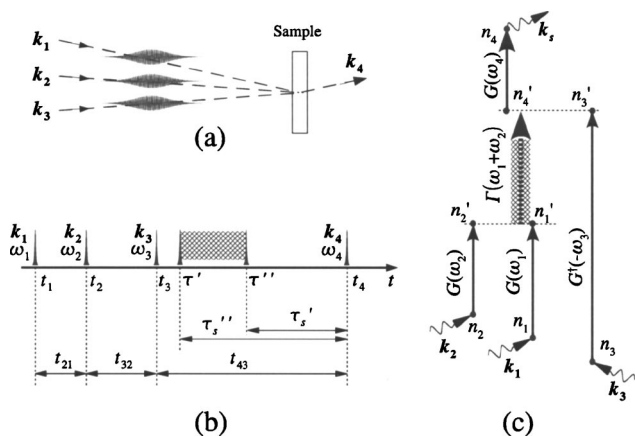


FIG. 1. (Color online) Third-order four-wave mixing experiment. The three incoming pulses with wave vectors \mathbf{k}_1 , \mathbf{k}_2 , and \mathbf{k}_3 generate a signal at $\mathbf{k}_4 = \pm\mathbf{k}_1 \pm \mathbf{k}_2 \pm \mathbf{k}_3$ (a). Interaction events and the definitions of time intervals in Eqs. (1), (C4), and (F3)–(F6) (b). Quasiparticle picture of the coherent response with respect to Eq. (26) (c). Three interactions with the optical fields (red points or peaks) create one-exciton particles. They evolve according to their Green's functions. The two excitons are scattered by Γ (blue dashed areas). Finally two excitons annihilate and the remaining exciton generates the signal.

CD is a good probe of molecular chirality: it has opposite signs for two enantiomers and vanishes for racemates—equal mixtures of two mirror structures.¹ CD of small molecules is usually described by including magnetic transition dipoles.^{3,4} However, large biological molecules such as DNA and proteins and chromophore aggregates (e.g., light harvesting systems) are spatially extended. Wave-vector-dependent terms, which go beyond the dipole approximation and are related to quadrupole and higher moments, become significant as the molecular size is increased. Local magnetic transition dipoles can be ignored for large molecules: the ratio of magnetic dipole and electric quadrupole moment is proportional to v/c , where v is the speed of electrons (for electronic transitions) or nuclei (for vibrational transitions) and c is the speed of light.⁴⁰ ECD for molecular aggregates was calculated to first order in wave vectors^{41,42} by modeling them as a collection of coupled electric dipoles. The dipole coordinates enter explicitly, showing high sensitivity to the geometry. This model has been successfully applied to biological light harvesting antenna system and recently to a large class of cylindrical aggregates.⁴³ A more general description of CD and optical rotation was developed using spatially non-local electric and magnetic optical response tensors.⁴⁴ Specific tensor elements of the linear response function (xy and yx), which is a second rank tensor, are responsible for CD. Nonlinear techniques which utilize circularly polarized optical fields, such as two-dimensional pump-probe were studied as well.^{45,46}

Third-order techniques performed with linearly polarized light (time and frequency resolved) are routinely used to probe isotropic systems. The experiment is depicted schematically in Fig. 1. The nonlinear response function $S^{(3)}$ is a fourth rank tensor,⁴⁷ which relates the third-order nonlinear polarization $\mathbf{P}^{(3)}$ to the optical field $\mathbf{E}(\mathbf{r}, t)$,

$$\mathbf{P}_{\nu_4}^{(3)}(\mathbf{r}_4, t_4) = \sum_{\nu_3 \nu_2 \nu_1} \int d\mathbf{r}_3 \int d\mathbf{r}_2 \int d\mathbf{r}_1 \int dt_3 \int dt_2 \int dt_1 S_{\nu_4, \nu_3 \nu_2 \nu_1}^{(3)}(\mathbf{r}_4 t_4, \mathbf{r}_3 t_3, \mathbf{r}_2 t_2, \mathbf{r}_1 t_1) \times \mathbf{E}_{\nu_3}(\mathbf{r}_3, t_3) \mathbf{E}_{\nu_2}(\mathbf{r}_2, t_2) \mathbf{E}_{\nu_1}(\mathbf{r}_1, t_1), \quad (1)$$

where $\nu = x, y, z$ denotes cartesian components. The polarization is measured at time t_4 and position \mathbf{r}_4 , while the \mathbf{r} integrations extend over the volume of a single molecule \mathcal{V} ($\int d\mathbf{r} \cdots = \int_V dx \int_V dy \int_V dz \cdots$) and time integrations are from $-\infty$ to $+\infty$. These integration limits are assumed throughout this paper unless they are otherwise specified. t_j with $j=1, 2, 3$ is the interaction time with the electric field \mathbf{E}_{ν_j} . Note that these time variables do not have a particular time ordering. The response function depends parametrically on both the coordinates of the system and the interaction times. It carries all material properties relevant for the optical response.

In general the third-order response function has 3^4 tensor elements. However, in the dipole approximation there are only three linearly independent components for isotropic systems:⁴⁸ $xyxy$, $xyyx$, and $xyyx$ ($xxxx$ is a linear combination of these elements). These have been successfully used for improving of spectral resolution in two-dimensional IR (2D IR) spectroscopies,^{49–53} however, they are not chirally-sensitive.

In this paper we go one step beyond the dipole approximation and calculate the first- and the third-order response function and the susceptibility, to first order in the optical wave vector. The finite tensor elements of third-order response tensors which contain an odd number of x (or y , or z such as $xxxy$, etc.) vanish for nonchiral molecules and are therefore chirally-sensitive. We use the nonlinear exciton equations (NEE) originally developed by Spano and Mukamel^{54–56} for four-wave mixing of coupled two-level^{57–60} and three-level^{61–63} molecules. The NEE were later extended to particles with arbitrary commutation relations and to Wannier excitons in semiconductors.⁶⁴ The equations establish an exciton scattering mechanism for the nonlinear response and avoid the expensive calculation of multiexciton eigenstates, which is a considerable advantage for large systems. Closed expressions are derived for infinite periodic systems, where translational symmetry may be employed to reduce the problem size. We apply our theory to α helical polypeptide in the amide I region.

In Sec. II we present the Hamiltonian and the NEE for vibrational excitons. In Sec. III we introduce the notation and parameters and calculate the linear susceptibility, recovering the well known expressions of linear absorption and circular dichroism. We then derive in Sec. IV expressions for the third-order susceptibility of oriented systems using the same assumptions and approximations, and extend them to isotropic ensembles in Sec. V using a universal tensor averaging procedure. Simplified expressions for periodic systems are derived in Sec. VI. The linear and the nonlinear signals are calculated for α and 3_{10} helices in Sec. VII. We pay particular attention to two-exciton resonance and compare the re-

sults within and beyond the dipole approximation. Various aspects of nonlinear spectroscopy beyond the dipole approximation are discussed in Sec. VIII.

Derivations of the expressions used in the main text are given in the Appendices. Appendix A introduces the exciton basis, the exciton Green's functions, and the scattering matrix. The reduced expressions for the scattering matrix for special models of nonlinearities are given in Appendix B. The optical response is derived from the NEE in Appendix C. General expressions for the susceptibilities in periodic systems are derived in Appendix D. Reduced scattering matrix expressions for periodic systems are given in Appendix E, and the time ordered optical response functions required for time-domain short pulse experiments are presented in Appendix F.

II. THE VIBRATIONAL EXCITON HAMILTONIAN AND THE NONLINEAR EXCITON EQUATIONS

We consider \mathcal{N} coupled anharmonic local vibrational modes described by the exciton Hamiltonian

$$\hat{H} = \sum_m \varepsilon_m \hat{B}_m^\dagger \hat{B}_m + \sum_{m \neq n} J_{m,n} \hat{B}_m^\dagger \hat{B}_n + \sum_{mn,m'n'} U_{mn,m'n'} \hat{B}_m^\dagger \hat{B}_n^\dagger \hat{B}_m \hat{B}_{n'} - \int d\mathbf{r} \hat{\mathbf{P}}(\mathbf{r}) \cdot \mathbf{E}(\mathbf{r}, t). \quad (2)$$

The creation, \hat{B}_m^\dagger , and annihilation, \hat{B}_m , operators for mode m satisfy the boson $[\hat{B}_m, \hat{B}_n^\dagger] = \delta_{mn}$ commutation relation. The first two terms represent the free-boson Hamiltonian: ε_m denotes the harmonic frequency of mode m and the quadratic intermode coupling, $J_{m,n}$, is calculated in the Heitler–London approximation where we neglect $\hat{B}_m^\dagger \hat{B}_n^\dagger$ and $\hat{B}_m \hat{B}_n$ terms. The third term represents a quartic anharmonicity and the fourth term is the interaction with the optical field $\mathbf{E}(\mathbf{r}, t)$ where

$$\hat{\mathbf{P}}(\mathbf{r}) = \sum_m \delta(\mathbf{r} - \mathbf{r}_m) \boldsymbol{\mu}_m (\hat{B}_m^\dagger + \hat{B}_m) \quad (3)$$

is the polarization operator and $\boldsymbol{\mu}_m$ is the transition dipole moment, a vector with the components $(\boldsymbol{\mu}_m^x, \boldsymbol{\mu}_m^y, \boldsymbol{\mu}_m^z)$, for mode m located at \mathbf{r}_m .

The expectation value of the polarization operator which describes the response of the system to the optical field will be calculated using the NEE.^{55,57,64} This hierarchy of equations of motion for exciton variables may be exactly truncated order by order in the field since the molecular Hamiltonian conserves the number of excitons and the optical field creates or annihilates one exciton at a time. By neglecting pure dephasing, the only required exciton variables for the third-order optical response are $B_m = \langle \hat{B}_m \rangle$ (one-exciton) and $Y_{mn} = \langle \hat{B}_m \hat{B}_n \rangle$ (two exciton). The NEE then assume the form^{55,56}

$$-i \frac{\partial B_m}{\partial t} + \sum_n h_{m,n} B_n = \mathcal{E}_m(t) - \sum_{l'm'n'} V_{ml'm'n'} B_{l'}^* Y_{m'n'}, \quad (4)$$

$$-i \frac{\partial Y_{mn}}{\partial t} + \sum_{m'n'} (h_{mn,m'n'}^{(Y)} + V_{mn,m'n'}) Y_{m'n'} = \mathcal{E}_m(t) B_n + \mathcal{E}_n(t) B_m. \quad (5)$$

Here $h_{m,n} = \delta_{m,n} \varepsilon_m + J_{m,n} (1 - \delta_{m,n})$ is an effective single exciton Hamiltonian, $h_{mn,m'n'}^{(Y)} = \delta_{m',m} h_{n,n'} + \delta_{n,n'} h_{m,m'}$ is a two-exciton Hamiltonian, $V_{mn,m'n'} = U_{mn,m'n'} + U_{nm,m'n'}$ is the anharmonicity matrix, and $\mathcal{E}_m(t) = \mathbf{E}(\mathbf{r}_m, t) \boldsymbol{\mu}_m$. The nonlinearities in these equations originate from the anharmonicity matrix. When it is neglected the two-exciton variables can be factorized as $Y_{mn} = B_m B_n$, Eq. (5) becomes redundant, Eq. (4) becomes linear and the nonlinear response vanishes. The polarization is given by the expectation value of Eq. (3)

$$\mathbf{P}(\mathbf{r}, t) = \sum_m \boldsymbol{\mu}_m (B_m(t) + B_m^*(t)) \delta(\mathbf{r} - \mathbf{r}_m). \quad (6)$$

Additional variables are required in the NEE when population transport and pure dephasing are included.⁶⁴ We shall calculate the nonlinear polarization and explore different limits of parameters using the Green's function solution of the NEE given in Appendix A.

III. LINEAR ABSORPTION AND CIRCULAR DICHROISM OF EXCITONS IN THE MOLECULAR FRAME

To introduce the notation and set the stage for calculating the nonlinear response we first review the nonlocal linear response. The nonlocal linear response function, $S_{\nu_2, \nu_1}^{(1)}(\mathbf{r}_2 t_2; \mathbf{r}_1 t_1)$, is defined by the following relation between the linear polarization $\mathbf{P}_{\nu_2}^{(1)}(\mathbf{r}_2, t_2)$ and the optical electric field $\mathbf{E}_{\nu_1}(\mathbf{r}_1 t_1)$:^{40,65,66}

$$\mathbf{P}_{\nu_2}^{(1)}(\mathbf{r}_2, t_2) = \sum_{\nu_1} \int d\mathbf{r}_1 \int dt_1 S_{\nu_2, \nu_1}^{(1)}(\mathbf{r}_2 t_2; \mathbf{r}_1 t_1) \mathbf{E}_{\nu_1}(\mathbf{r}_1 t_1). \quad (7)$$

The linear susceptibility relates these quantities in the frequency/momentum domain,

$$\mathbf{P}_{\nu_2}^{(1)}(\mathbf{k}_2, \omega_2) = \frac{1}{(2\pi)^4} \sum_{\nu_1} \int d\mathbf{k}_1 \int d\omega_1 \chi_{\nu_2, \nu_1}^{(1)}(-\mathbf{k}_2 - \omega_2; \mathbf{k}_1 \omega_1) \mathbf{E}_{\nu_1}(\mathbf{k}_1 \omega_1), \quad (8)$$

where we use the following convention for the Fourier transform

$$F(\mathbf{k}, \omega) = \int d\mathbf{r} \int dt F(\mathbf{r}, t) \exp(i\mathbf{k}\mathbf{r} + i\omega t). \quad (9)$$

The susceptibility and the response function are connected by

$$\begin{aligned} & \chi_{\nu_2, \nu_1}^{(1)}(-\mathbf{k}_2 - \omega_2; \mathbf{k}_1 \omega_1) \\ &= \int_{\nu} d\mathbf{r}_2 \int_{\nu} d\mathbf{r}_1 \int dt_2 \int dt_1 S_{\nu_2, \nu_1}^{(1)}(\mathbf{r}_2 t_2; \mathbf{r}_1 t_1) \\ & \quad \times \exp(i\mathbf{k}_2 \mathbf{r}_2 - i\mathbf{k}_1 \mathbf{r}_1 + i\omega_2 t_2 - i\omega_1 t_1). \end{aligned} \quad (10)$$

Using Eqs. (C1), (7), and (3), the linear response function for our model is given by

$$S_{\nu_2, \nu_1}^{(1)}(\mathbf{r}_2 t_2; \mathbf{r}_1 t_1) = i \sum_{mn} \delta(\mathbf{r}_2 - \mathbf{r}_m) \delta(\mathbf{r}_1 - \mathbf{r}_n) \boldsymbol{\mu}_m^{\nu_2} \boldsymbol{\mu}_n^{\nu_1} \times G_{mn}(t_2 - t_1) + c. c., \quad (11)$$

where $G(t)$ is the single exciton Green's function [Eq. (A4)] and c.c. denotes the complex conjugate. From Eqs. (10) and (11) we obtain the susceptibility

$$\begin{aligned} \chi_{\nu_2, \nu_1}^{(1)}(-\mathbf{k}_2 - \omega_2; \mathbf{k}_1 \omega_1) &= 2\pi i \delta(\omega_2 - \omega_1) \\ &\times \sum_{mn} \exp(i\mathbf{k}_2 \mathbf{r}_m - i\mathbf{k}_1 \mathbf{r}_n) \boldsymbol{\mu}_m^{\nu_2} \boldsymbol{\mu}_n^{\nu_1} G_{mn}(\omega_1) \\ &+ c. c., \end{aligned} \quad (12)$$

where c.c.' stands for complex conjugate with reversing the signs of momentum and frequency: $\mathbf{k} \rightarrow -\mathbf{k}$ and $\omega \rightarrow -\omega$, and $G(\omega)$ is the frequency domain Green's function given by Eq. (A6). Time translational invariance implies that $\omega_2 = \omega_1$. For uniform systems with space translational symmetry we have $\mathbf{k}_2 = \mathbf{k}_1$.

Using the exciton basis $\psi_{\xi m}$ (eigenstates of the single exciton block of the molecular Hamiltonian) defined in Eq. (A1), Eq. (11) reads

$$S_{\nu_2, \nu_1}^{(1)}(\mathbf{r}_2 t_2; \mathbf{r}_1 t_1) = i \sum_{\xi} \mathbf{d}_{\xi}^{\nu_2}(\mathbf{r}_2) \mathbf{d}_{\xi}^{\nu_1*}(\mathbf{r}_1) I_{\xi}(t_2 - t_1) + c. c., \quad (13)$$

where the sum now runs over the one-exciton eigenstates ξ and $I_{\xi}(t)$ is the single exciton Green's function,

$$I_{\xi}(t) = \theta(t) \exp(-i\Omega_{\xi} t - \gamma_{\xi} t), \quad (14)$$

where Ω_{ξ} and γ_{ξ} are the frequency and dephasing rate of the ξ exciton state, respectively, $\theta(t)$ is the Heaviside step function ($\theta(t) = 0$ for $t < 0$ and $\theta(t) = 1$ for $t \geq 0$) and the transition dipole is

$$\mathbf{d}_{\xi}^{\nu}(\mathbf{r}) = \sum_m \delta(\mathbf{r} - \mathbf{r}_m) \boldsymbol{\mu}_m^{\nu} \psi_{\xi m}. \quad (15)$$

The susceptibility is similarly given by

$$\begin{aligned} \chi_{\nu_2, \nu_1}^{(1)}(-\mathbf{k}_2 - \omega_2; \mathbf{k}_1 \omega_1) &= 2\pi i \delta(\omega_2 - \omega_1) \sum_{\xi} \mathbf{d}_{\xi}^{\nu_2}(\mathbf{k}_2) \mathbf{d}_{\xi}^{\nu_1*}(\mathbf{k}_1) I_{\xi}(\omega_1) + c. c., \end{aligned} \quad (16)$$

where, the nonlocal exciton transition dipoles are transformed to momentum space

$$\mathbf{d}_{\xi}^{\nu}(\mathbf{k}) = \sum_m e^{i\mathbf{k} \mathbf{r}_m} \boldsymbol{\mu}_m^{\nu} \psi_{\xi m} \quad (17)$$

and the frequency domain Green's function

$$I_{\xi}(\omega) = \frac{i}{\omega - \Omega_{\xi} + i\gamma_{\xi}} \quad (18)$$

is the Fourier transform of Eq. (14).

The linear response function (and the susceptibility) describes all linear properties of an ensemble of oriented molecules in the lab frame.

The linear absorption of the field is given by^{67,68}

$$\sigma_A = \int d\mathbf{r} \int dt \left(\sum_{\nu} \frac{\partial \mathbf{P}_{\nu}^{(1)}(\mathbf{r}, t)}{\partial t} \cdot \mathbf{E}_{\nu}(\mathbf{r}, t) \right), \quad (19)$$

Transforming to the momentum/frequency domain we obtain

$$\sigma_A = \frac{-i}{(2\pi)^4} \int d\mathbf{k} \int \omega d\omega \sum_{\nu} \mathbf{E}_{\nu}(-\mathbf{k}, -\omega) \mathbf{P}_{\nu}^{(1)}(\mathbf{k}, \omega). \quad (20)$$

We next consider a monochromatic optical field

$$\mathbf{E}(\mathbf{r}, t) = \frac{1}{2} E_0 (\mathbf{e}^{\nu_1} + a \mathbf{e}^{\nu_2} e^{-i\phi_0}) \exp(i\mathbf{k}_0 \mathbf{r} - i\omega_0 t) + c. c. \quad (21)$$

Here \mathbf{e}^{ν} is a unit vector along $\nu = x, y, z$, a is a ratio of two perpendicular amplitudes along ν_1 and ν_2 , ϕ_0 is a phase difference between them and E_0 is the overall amplitude. The vectors \mathbf{e}^{ν_1} , \mathbf{e}^{ν_2} , \mathbf{k}_0 form a right-handed orthogonal axis system. Equation (21) represents linearly polarized light along \mathbf{e}^{ν_1} when $a=0$; right-handed circularly polarized light when $a=1$ and $\phi_0 = +\pi/2$ and left-handed with $a=1$ and $\phi_0 = -\pi/2$. Combining Eq. (8), (20), and (21), we obtain for the linear absorption

$$\begin{aligned} \sigma_A(\omega_0) &= i \frac{E_0^2 \omega_0}{4} [\chi_{\nu_1 \nu_1}^{(1)}(-\mathbf{k}_0, \omega_0; \mathbf{k}_0, -\omega_0) - \chi_{\nu_1 \nu_1}^{(1)}(\mathbf{k}_0, -\omega_0; -\mathbf{k}_0, \omega_0) + a^2 \chi_{\nu_2 \nu_2}^{(1)}(-\mathbf{k}_0, \omega_0; \mathbf{k}_0, -\omega_0) - a^2 \chi_{\nu_2 \nu_2}^{(1)}(\mathbf{k}_0, -\omega_0; -\mathbf{k}_0, \omega_0) \\ &+ a e^{i\phi_0} \chi_{\nu_1 \nu_2}^{(1)}(-\mathbf{k}_0, \omega_0; \mathbf{k}_0, -\omega_0) - a e^{-i\phi_0} \chi_{\nu_1 \nu_2}^{(1)}(\mathbf{k}_0, -\omega_0; -\mathbf{k}_0, \omega_0) + a e^{-i\phi_0} \chi_{\nu_2 \nu_1}^{(1)}(-\mathbf{k}_0, \omega_0; \mathbf{k}_0, -\omega_0) \\ &- a e^{i\phi_0} \chi_{\nu_2 \nu_1}^{(1)}(\mathbf{k}_0, -\omega_0; -\mathbf{k}_0, \omega_0)]. \end{aligned} \quad (22)$$

By setting $a=0$ we obtain the absorption of linearly polarized light. The circular dichroism spectrum is defined as a difference of absorption of left-circularly polarized light ($a=1$, $\phi_0 = -\pi/2$) and right-circularly polarized light ($a=1$, $\phi_0 = \pi/2$),

$$\sigma_{CD}(\omega_0) = -i \frac{E_0^2 \omega_0}{2} [i \chi_{\nu_1 \nu_2}^{(1)}(-\mathbf{k}_0, \omega_0; \mathbf{k}_0, -\omega_0) + i \chi_{\nu_1 \nu_2}^{(1)}(\mathbf{k}_0, -\omega_0; -\mathbf{k}_0, \omega_0) - i \chi_{\nu_2 \nu_1}^{(1)}(-\mathbf{k}_0, \omega_0; \mathbf{k}_0, -\omega_0) - i \chi_{\nu_2 \nu_1}^{(1)}(\mathbf{k}_0, -\omega_0; -\mathbf{k}_0, \omega_0)]. \quad (23)$$

The linear absorption (circular dichroism) depends on diagonal (off diagonal) tensor components of the response function. Setting $\nu_1=x$, $\nu_2=y$ giving $\mathbf{k}_0=\mathbf{e}^z k_z$, the absorption of a linearly polarized light is

$$\sigma_A(\omega_0) = 2\pi \frac{E_0^2 \omega_0}{4} \sum_{mn} \boldsymbol{\mu}_m^x \boldsymbol{\mu}_n^x \text{Re}[\exp(-ik_z \mathbf{r}_{mn}^z) G_{mn}(\omega_0)]$$

and the circular dichroism signal

$$\sigma_{CD}(\omega_0) = 2\pi \frac{E_0^2 \omega_0}{2} \sum_{mn} [\boldsymbol{\mu}_m \times \boldsymbol{\mu}_n]_z \times \text{Re}[i \exp(-ik_z \mathbf{r}_{mn}^z) G_{mn}(\omega_0)].$$

These results are exact for coupled dipoles with arbitrary geometry and a fixed orientation with respect to the optical field.

IV. NONLOCAL THIRD-ORDER RESPONSE FUNCTION IN THE MOLECULAR FRAME

Four-wave-mixing processes are described by the third-order polarization,⁴⁰

$$\begin{aligned} \mathbf{P}_{\nu_4}^{(3)}(\mathbf{k}_4, \omega_4) &= \frac{1}{(2\pi)^{12}} \sum_{\nu_3 \nu_2 \nu_1} \int d\mathbf{k}_3 \int d\omega_3 \int d\mathbf{k}_2 \int d\omega_2 \\ &\int d\mathbf{k}_1 \int d\omega_1 \chi_{\nu_4, \nu_3 \nu_2 \nu_1}^{(3)}(-\mathbf{k}_4 - \omega_4; \mathbf{k}_3 \omega_3, \mathbf{k}_2 \omega_2, \mathbf{k}_1 \omega_1) \\ &\times \mathbf{E}_{\nu_3}(\mathbf{k}_3, \omega_3) \mathbf{E}_{\nu_2}(\mathbf{k}_2, \omega_2) \mathbf{E}_{\nu_1}(\mathbf{k}_1, \omega_1). \end{aligned} \quad (24)$$

The susceptibility [Eq. (24)] and the response function [Eq. (1)] are connected by

$$\begin{aligned} \chi_{\nu_4, \nu_3 \nu_2 \nu_1}^{(3)}(-\mathbf{k}_4 - \omega_4; \mathbf{k}_3 \omega_3, \mathbf{k}_2 \omega_2, \mathbf{k}_1 \omega_1) &= \int d\mathbf{r}_4 \int dt_4 \int d\mathbf{r}_3 \int dt_3 \int d\mathbf{r}_2 \int dt_2 \int d\mathbf{r}_1 \int dt_1 \\ &S_{\nu_4, \nu_3 \nu_2 \nu_1}^{(3)}(\mathbf{r}_4 t_4, \mathbf{r}_3 t_3, \mathbf{r}_2 t_2, \mathbf{r}_1 t_1) \\ &\times \exp\left[i(\mathbf{k}_4 \mathbf{r}_4 + \omega_4 t_4) - i \sum_l^3 (\mathbf{k}_l \mathbf{r}_l + \omega_l t_l)\right]. \end{aligned} \quad (25)$$

The response function is directly observed in time domain experiments with ultrashort optical pulses where the time integration in Eq. (1) can be eliminated whereas the susceptibility is observed in the opposite CW limit when the ω integrations in Eq. (24) can be eliminated.

A Green's function expression for $S^{(3)}$ obtained by solving the NEE is given in Eq. (C4). Applying the transform of Eq. (25) we obtain

$$\begin{aligned} \chi_{\nu_4, \nu_3 \nu_2 \nu_1}^{(3)}(-\mathbf{k}_4, -\omega_4; \mathbf{k}_3, \omega_3, \mathbf{k}_2, \omega_2, \mathbf{k}_1, \omega_1) &= 2\pi i \delta(\omega_4 - \omega_3 - \omega_2 - \omega_1) \mathcal{P}_{i\mathbf{k}\omega} \\ &\times \sum_{n_4 n_3 n_2 n_1} \exp(i\mathbf{k}_4 \mathbf{r}_{n_4} - i\mathbf{k}_3 \mathbf{r}_{n_3} - i\mathbf{k}_2 \mathbf{r}_{n_2} - i\mathbf{k}_1 \mathbf{r}_{n_1}) \mathbf{M}_{n_4 n_3 n_2 n_1}^{\nu_4 \nu_3 \nu_2 \nu_1} \\ &\times \sum_{n'_4 n'_3 n'_2 n'_1} \Gamma_{n'_4 n'_3 n'_2 n'_1}(\omega_1 + \omega_2) G_{n_4 n'_4}(\omega_4) G_{n'_3 n_3}^\dagger(-\omega_3) \\ &\times G_{n'_2 n_2}(\omega_2) G_{n'_1 n_1}(\omega_1) + \text{c. c.}', \end{aligned} \quad (26)$$

where the frequency domain Green's functions $G(\omega)$ and the scattering matrix $\Gamma(\omega)$ are given by Eqs. (18) and (A16), respectively. $\mathbf{M}_{n_4 n_3 n_2 n_1}^{\nu_4 \nu_3 \nu_2 \nu_1} = \boldsymbol{\mu}_{n_4}^{\nu_4} \boldsymbol{\mu}_{n_3}^{\nu_3} \boldsymbol{\mu}_{n_2}^{\nu_2} \boldsymbol{\mu}_{n_1}^{\nu_1}$ is the orientational tensor and $\mathcal{P}_{i\mathbf{k}\omega}$ denotes the sum over the six permutations of $\nu_1 \mathbf{k}_1 \omega_1$, $\nu_2 \mathbf{k}_2 \omega_2$, and $\nu_3 \mathbf{k}_3 \omega_3$. Since $\chi^{(3)}$ is already symmetric with respect to 1 and 2 we only need to permute 1 with 3 and 2 with 3. We therefore need only three permutations.

Equation (26) leads to the following physical picture for the response.⁶⁴ Each of the three optical fields interacts with the system at points $n_1 t_1$, $n_2 t_2$, and $n_3 t_3$ as shown in Fig. 1. The two excitons generated at points n_1 and n_2 have positive frequency and evolve independently to n'_1 and n'_2 where they are scattered, changing their positions to n'_3 and n'_4 . The exciton at n'_4 evolves to n_4 and generates the signal, while the exciton generated at n'_3 evolves to n_3 and is annihilated by the third field. In this representation the scattering matrix is the only source for the nonlinear polarization. For harmonic oscillators the matrix V , the scattering matrix, and, consequently, $\chi^{(3)}$ vanish. The susceptibility depends on the orientation of the molecule in the laboratory frame and has a nontrivial dependence on the wave vectors.

In the exciton basis [Eq. (A1)] we substitute Eq. (A4) into Eq. (26) to obtain

$$\begin{aligned} \chi_{\nu_4, \nu_3 \nu_2 \nu_1}^{(3)}(-\mathbf{k}_4, -\omega_4; \mathbf{k}_3, \omega_3, \mathbf{k}_2, \omega_2, \mathbf{k}_1, \omega_1) &= 2\pi i \delta(\omega_4 - \omega_3 - \omega_2 - \omega_1) \mathcal{P}_{i\mathbf{k}\omega} \\ &\times \sum_{\xi_4 \xi_3 \xi_2 \xi_1} d_{\xi_4}^{\nu_4}(\mathbf{k}_4) d_{\xi_3}^{\nu_3}(-\mathbf{k}_3) d_{\xi_2}^{\nu_2}(\mathbf{k}_2) d_{\xi_1}^{\nu_1}(\mathbf{k}_1) \\ &\times \Gamma_{\xi_4 \xi_3, \xi_2 \xi_1}(\omega_2 + \omega_1) I_{\xi_4}(\omega_4) I_{\xi_3}^*(-\omega_3) \\ &\times I_{\xi_2}(\omega_2) I_{\xi_1}(\omega_1) + \text{c. c.}', \end{aligned} \quad (27)$$

where the exciton transition dipoles were defined in Eq. (17), the exciton Green's function in the eigenstate basis is given by Eq. (18) and the scattering matrix $\Gamma(\omega)$ is obtained by the Fourier transform of Eq. (C6).

V. THE RESPONSE OF ISOTROPIC ENSEMBLES

The optical fields, wave vectors, and space coordinates are defined in the lab frame, while the transition dipoles and their position vectors are given in the molecular frame. Rotational averaging, $\langle \cdots \rangle$, needs to be performed over the relative orientation of the two frames to calculate the response functions for isotropic (randomly oriented) ensembles of molecules.⁴⁸ Equation (16) then becomes

$$\begin{aligned} \chi_{\nu_2, \nu_1}^{(1)}(-\mathbf{k}_2 - \omega_2; \mathbf{k}_1 \omega_1) &= 2\pi i \delta(\omega_2 - \omega_1) \\ &\times \sum_{\xi} \langle d_{\xi}^{\nu_2}(\mathbf{k}_2) d_{\xi}^{\nu_1*}(\mathbf{k}_1) \rangle I_{\xi}(\omega_1) \\ &+ \text{c. c.}', \end{aligned} \quad (28)$$

with

$$\langle d_{\xi}^{\nu_2}(\mathbf{k}_2) d_{\xi}^{\nu_1*}(\mathbf{k}_1) \rangle = \sum_{n_2 n_1} \psi_{\xi n_2} \psi_{\xi n_1}^* \langle e^{i\mathbf{k}_2 \mathbf{r}_{n_2} - i\mathbf{k}_1 \mathbf{r}_{n_1}} \boldsymbol{\mu}_{n_2}^{\nu_2} \boldsymbol{\mu}_{n_1}^{\nu_1} \rangle, \quad (29)$$

\mathbf{k}_i , and the tensor components ν_i are lab frame quantities, while the transition dipoles $\boldsymbol{\mu}_n$ and coordinates \mathbf{r}_n are molecular properties defined in the molecular frame. This type of averaging required for μm size macromolecules was calculated by Craig and Thirunamachandran for linear absorption and for CD.⁶⁹

For an isotropic ensemble of molecules we should treat each molecule as identical system with its collection of transition dipoles having unique orientation with respect to the lab frame. The coordinate of each mode in the lab frame depends on the position of the molecule. Therefore, in general we should replace the coordinates \mathbf{r}_m with $\mathcal{R} + \mathbf{r}_m$, where \mathcal{R} is the molecular position (an origin of the molecular coordinate system) in the lab frame and \mathbf{r}_m is the coordinate of mode m with respect to that origin. Taking into account the positions of molecules in the ensemble, factors such as $\exp(i\mathbf{k}_2 \mathbf{r}_{n_2} - i\mathbf{k}_1 \mathbf{r}_{n_1})$ will change to $\exp(i\mathcal{R}(\mathbf{k}_2 - \mathbf{k}_1)) \exp(i\mathbf{k}_2 \mathbf{r}_{n_2} - i\mathbf{k}_1 \mathbf{r}_{n_1})$, where now $\exp(i\mathcal{R}(\mathbf{k}_2 - \mathbf{k}_1))$ is an overall phase factor which leads to phase-matching condition for the optical fields when integrated over an isotropic bulk sample. The second factor, $\exp(i\mathbf{k}_2 \mathbf{r}_{n_2} - i\mathbf{k}_1 \mathbf{r}_{n_1})$, is now responsible for the variation of phase within the molecule. Hereafter we keep the phase-matching condition and neglect the $\exp(i\mathcal{R}(\mathbf{k}_2 - \mathbf{k}_1))$ factor. The coordinates \mathbf{r}_m vary only within one molecule and for molecules smaller than the wavelength of light we have $\mathbf{k} \mathbf{r}_m \ll 1$, and the exponential functions in Eq. (29) can be expanded to first order,

$$\begin{aligned} \langle e^{i\mathbf{k}_2 \mathbf{r}_{n_2} - i\mathbf{k}_1 \mathbf{r}_{n_1}} \boldsymbol{\mu}_{n_2}^{\nu_2} \boldsymbol{\mu}_{n_1}^{\nu_1} \rangle &= \langle \boldsymbol{\mu}_{n_2}^{\nu_2} \boldsymbol{\mu}_{n_1}^{\nu_1} \rangle + i \sum_{\kappa} \mathbf{k}_2^{\kappa} \langle \mathbf{r}_{n_2}^{\kappa} \boldsymbol{\mu}_{n_2}^{\nu_2} \boldsymbol{\mu}_{n_1}^{\nu_1} \rangle \\ &- i \sum_{\kappa} \mathbf{k}_1^{\kappa} \langle \mathbf{r}_{n_1}^{\kappa} \boldsymbol{\mu}_{n_2}^{\nu_2} \boldsymbol{\mu}_{n_1}^{\nu_1} \rangle, \end{aligned} \quad (30)$$

where $\kappa = x, y, z$. This expansion allows to transform vectors back to the exciton basis. Substituting Eq. (30) in Eq. (29) and performing the summations over modes we obtain

$$\begin{aligned} \langle d_{\xi}^{\nu_2}(\mathbf{k}_2) d_{\xi}^{\nu_1*}(\mathbf{k}_1) \rangle &= \langle d_{\xi}^{\nu_2} d_{\xi}^{\nu_1*} \rangle + i \sum_{\kappa} \mathbf{k}_2^{\kappa} \langle \bar{d}_{\xi}^{\kappa, \nu_2} d_{\xi}^{\nu_1*} \rangle \\ &- i \sum_{\kappa} \mathbf{k}_1^{\kappa} \langle \bar{d}_{\xi}^{\kappa, \nu_1} d_{\xi}^{\nu_2*} \rangle, \end{aligned} \quad (31)$$

where we had defined the transition dipole vector for the zero momentum exciton state

$$\mathbf{d}_{\xi}^{\nu} \equiv d_{\xi}^{\nu}(\mathbf{k} = 0) = \sum_m \boldsymbol{\mu}_m^{\nu} \psi_{\xi, m}, \quad (32)$$

and the tensor

$$\bar{\mathbf{d}}_{\xi}^{\kappa, \nu} = \sum_m \mathbf{r}_m^{\kappa} \boldsymbol{\mu}_m^{\nu} \psi_{\xi, m}. \quad (33)$$

Proceeding along the same steps we obtain average third-order response. Rotational averaging of Eq. (27) gives

$$\begin{aligned} \chi_{\nu_4, \nu_3, \nu_2, \nu_1}^{(3)}(-\mathbf{k}_4, -\omega_4; \mathbf{k}_3, \omega_3, \mathbf{k}_2, \omega_2, \mathbf{k}_1, \omega_1) &= 2\pi i \delta(\omega_4 - \omega_3 - \omega_2 - \omega_1) \mathcal{P}_{i\mathbf{k}\omega} \sum_{\xi_4 \xi_3 \xi_2 \xi_1} \langle d_{\xi_4}^{\nu_4}(\mathbf{k}_4) d_{\xi_3}^{\nu_3}(-\mathbf{k}_3) \\ &\times d_{\xi_2}^{\nu_2}(\mathbf{k}_2) d_{\xi_1}^{\nu_1*}(\mathbf{k}_1) \rangle \Gamma_{\xi_4 \xi_3, \xi_2 \xi_1}(\omega_2 + \omega_1) I_{\xi_4}(\omega_4) \\ &\times I_{\xi_3}^*(-\omega_3) I_{\xi_2}(\omega_2) I_{\xi_1}(\omega_1) + \text{c. c.}', \end{aligned} \quad (34)$$

with

$$\begin{aligned} \langle d_{\xi_4}^{\nu_4}(\mathbf{k}_4) d_{\xi_3}^{\nu_3}(-\mathbf{k}_3) d_{\xi_2}^{\nu_2}(\mathbf{k}_2) d_{\xi_1}^{\nu_1*}(\mathbf{k}_1) \rangle &= \sum_{n_4 n_3 n_2 n_1} \psi_{\xi_4 n_4} \psi_{\xi_3 n_3} \psi_{\xi_2 n_2}^* \psi_{\xi_1 n_1}^* \\ &\times \langle e^{i\mathbf{k}_4 \mathbf{r}_{n_4} - i\mathbf{k}_3 \mathbf{r}_{n_3} - i\mathbf{k}_2 \mathbf{r}_{n_2} - i\mathbf{k}_1 \mathbf{r}_{n_1}} \boldsymbol{\mu}_{n_4}^{\nu_4} \boldsymbol{\mu}_{n_3}^{\nu_3} \boldsymbol{\mu}_{n_2}^{\nu_2} \boldsymbol{\mu}_{n_1}^{\nu_1} \rangle, \end{aligned} \quad (35)$$

where

$$\begin{aligned} \langle e^{i\mathbf{k}_4 \mathbf{r}_{n_4} - i\mathbf{k}_3 \mathbf{r}_{n_3} - i\mathbf{k}_2 \mathbf{r}_{n_2} - i\mathbf{k}_1 \mathbf{r}_{n_1}} \boldsymbol{\mu}_{n_4}^{\nu_4} \boldsymbol{\mu}_{n_3}^{\nu_3} \boldsymbol{\mu}_{n_2}^{\nu_2} \boldsymbol{\mu}_{n_1}^{\nu_1} \rangle &= \langle \boldsymbol{\mu}_{n_4}^{\nu_4} \boldsymbol{\mu}_{n_3}^{\nu_3} \boldsymbol{\mu}_{n_2}^{\nu_2} \boldsymbol{\mu}_{n_1}^{\nu_1} \rangle + i \sum_{\kappa} \mathbf{k}_4^{\kappa} \langle \mathbf{r}_{n_4}^{\kappa} \boldsymbol{\mu}_{n_4}^{\nu_4} \boldsymbol{\mu}_{n_3}^{\nu_3} \boldsymbol{\mu}_{n_2}^{\nu_2} \boldsymbol{\mu}_{n_1}^{\nu_1} \rangle \\ &- i \sum_{\kappa} \mathbf{k}_3^{\kappa} \langle \mathbf{r}_{n_3}^{\kappa} \boldsymbol{\mu}_{n_4}^{\nu_4} \boldsymbol{\mu}_{n_3}^{\nu_3} \boldsymbol{\mu}_{n_2}^{\nu_2} \boldsymbol{\mu}_{n_1}^{\nu_1} \rangle \\ &- i \sum_{\kappa} \mathbf{k}_2^{\kappa} \langle \mathbf{r}_{n_2}^{\kappa} \boldsymbol{\mu}_{n_4}^{\nu_4} \boldsymbol{\mu}_{n_3}^{\nu_3} \boldsymbol{\mu}_{n_2}^{\nu_2} \boldsymbol{\mu}_{n_1}^{\nu_1} \rangle \\ &- i \sum_{\kappa} \mathbf{k}_1^{\kappa} \langle \mathbf{r}_{n_1}^{\kappa} \boldsymbol{\mu}_{n_4}^{\nu_4} \boldsymbol{\mu}_{n_3}^{\nu_3} \boldsymbol{\mu}_{n_2}^{\nu_2} \boldsymbol{\mu}_{n_1}^{\nu_1} \rangle. \end{aligned} \quad (36)$$

In the exciton basis we finally obtain

$$\begin{aligned} \langle d_{\xi_4}^{\nu_4}(\mathbf{k}_4) d_{\xi_3}^{\nu_3}(-\mathbf{k}_3) d_{\xi_2}^{\nu_2}(\mathbf{k}_2) d_{\xi_1}^{\nu_1*}(\mathbf{k}_1) \rangle &= \langle d_{\xi_4}^{\nu_4} d_{\xi_3}^{\nu_3} d_{\xi_2}^{\nu_2} d_{\xi_1}^{\nu_1*} \rangle \\ &+ i \sum_{\kappa} \mathbf{k}_4^{\kappa} \langle \bar{d}_{\xi_4}^{\kappa, \nu_4} d_{\xi_3}^{\nu_3} d_{\xi_2}^{\nu_2} d_{\xi_1}^{\nu_1*} \rangle - i \sum_{\kappa} \mathbf{k}_3^{\kappa} \langle \bar{d}_{\xi_3}^{\kappa, \nu_3} d_{\xi_4}^{\nu_4} d_{\xi_2}^{\nu_2} d_{\xi_1}^{\nu_1*} \rangle \\ &- i \sum_{\kappa} \mathbf{k}_2^{\kappa} \langle \bar{d}_{\xi_2}^{\kappa, \nu_2} d_{\xi_3}^{\nu_3} d_{\xi_4}^{\nu_4} d_{\xi_1}^{\nu_1*} \rangle \\ &- i \sum_{\kappa} \mathbf{k}_1^{\kappa} \langle \bar{d}_{\xi_1}^{\kappa, \nu_1} d_{\xi_3}^{\nu_3} d_{\xi_2}^{\nu_2} d_{\xi_4}^{\nu_4} \rangle, \end{aligned} \quad (37)$$

Eqs. (31) and (37) require second to fifth rank rotational averagings. The first terms in these equations correspond to the dipole approximation. The remaining terms which contain the transition dipole and a coordinate represent a first-order correction to the dipole approximation. These terms do not depend on the coordinate origin of the molecular frame provided $\mathbf{k}_4 = \mathbf{k}_3 + \mathbf{k}_2 + \mathbf{k}_1$, which is the phase-matching condition.

The projection of a molecular vector such as \mathbf{r}_m or $\boldsymbol{\mu}_m$ onto the lab coordinate system can be represented as a scalar product $\mathbf{e}^{\nu} \cdot \mathbf{r}_m$ (and $\mathbf{e}^{\nu} \cdot \boldsymbol{\mu}_m$), where \mathbf{e}^{ν} is a unit vector in the lab frame. These products have simple transformations between coordinate systems, and rotational averages can be

TABLE I. Isotropic rotational average tensors (Ref. 48). $\epsilon_{\alpha_3\alpha_2\alpha_1}$ is the antisymmetric Levi-Civita tensor: $\epsilon_{\alpha_3\alpha_2\alpha_1}$ is equal to 1 for $(\alpha_3, \alpha_2, \alpha_1) = (xyz), (yxz), (zxy)$, -1 for $(\alpha_3, \alpha_2, \alpha_1) = (xzy), (yxz), (zyx)$, and 0 otherwise.

Tensor element	Value
$\mathbf{T}_{\nu_2\nu_1, \alpha_2\alpha_1}^{(2)}$	$\frac{1}{3}\delta_{\nu_2\nu_1}\delta_{\alpha_2\alpha_1}$
$\mathbf{T}_{\nu_3\nu_2\nu_1, \alpha_3\alpha_2\alpha_1}^{(3)}$	$\frac{1}{6}\epsilon_{\nu_3\nu_2\nu_1}\epsilon_{\alpha_3\alpha_2\alpha_1}$
$\mathbf{T}_{\nu_4\nu_3\nu_2\nu_1, \alpha_4\alpha_3\alpha_2\alpha_1}^{(4)}$	$\frac{1}{30}\begin{pmatrix} \delta_{\nu_4\nu_3}\delta_{\nu_2\nu_1} \\ \delta_{\nu_4\nu_2}\delta_{\nu_3\nu_1} \\ \delta_{\nu_4\nu_1}\delta_{\nu_3\nu_2} \end{pmatrix}^T \begin{pmatrix} 4 & -1 & -1 \\ -1 & 4 & -1 \\ -1 & -1 & 4 \end{pmatrix} \begin{pmatrix} \delta_{\alpha_4\alpha_3}\delta_{\alpha_2\alpha_1} \\ \delta_{\alpha_4\alpha_2}\delta_{\alpha_3\alpha_1} \\ \delta_{\alpha_4\alpha_1}\delta_{\alpha_3\alpha_2} \end{pmatrix}$
$\mathbf{T}_{\nu_5\nu_4\nu_3\nu_2\nu_1, \alpha_5\alpha_4\alpha_3\alpha_2\alpha_1}^{(5)}$	$\frac{1}{30}\begin{pmatrix} \epsilon_{\nu_5\nu_4\nu_3}\delta_{\nu_2\nu_1} \\ \epsilon_{\nu_5\nu_4\nu_2}\delta_{\nu_3\nu_1} \\ \epsilon_{\nu_5\nu_4\nu_1}\delta_{\nu_3\nu_2} \\ \epsilon_{\nu_5\nu_3\nu_2}\delta_{\nu_4\nu_1} \\ \epsilon_{\nu_5\nu_3\nu_1}\delta_{\nu_4\nu_2} \\ \epsilon_{\nu_5\nu_2\nu_1}\delta_{\nu_4\nu_3} \end{pmatrix}^T \begin{pmatrix} 3 & -1 & -1 & 1 & 1 & 0 \\ -1 & 3 & -1 & -1 & 0 & 1 \\ -1 & -1 & 3 & 0 & -1 & -1 \\ 1 & -1 & 0 & 3 & -1 & 1 \\ 1 & 0 & -1 & -1 & 3 & -1 \\ 0 & 1 & -1 & 1 & -1 & 3 \end{pmatrix} \begin{pmatrix} \epsilon_{\alpha_5\alpha_4\alpha_3}\delta_{\alpha_2\alpha_1} \\ \epsilon_{\alpha_5\alpha_4\alpha_2}\delta_{\alpha_3\alpha_1} \\ \epsilon_{\alpha_5\alpha_4\alpha_1}\delta_{\alpha_3\alpha_2} \\ \epsilon_{\alpha_5\alpha_3\alpha_2}\delta_{\alpha_4\alpha_1} \\ \epsilon_{\alpha_5\alpha_3\alpha_1}\delta_{\alpha_4\alpha_2} \\ \epsilon_{\alpha_5\alpha_2\alpha_1}\delta_{\alpha_4\alpha_3} \end{pmatrix}$

easily calculated. For an s th rank product of any system vectors \mathbf{a} we have the following transformation¹ between the molecular and the lab frames:

$$\langle \mathbf{a}_s^{\nu_s} \cdots \mathbf{a}_1^{\nu_1} \rangle \equiv \langle (\mathbf{e}^{\nu_s} \cdot \mathbf{a}_s) \cdots (\mathbf{e}^{\nu_1} \cdot \mathbf{a}_1) \rangle \\ = \sum_{\alpha_s \cdots \alpha_1} \mathbf{T}_{\nu_s \cdots \nu_1, \alpha_s \cdots \alpha_1}^{(s)} \mathbf{a}_s^{\alpha_s} \cdots \mathbf{a}_1^{\alpha_1}, \quad (38)$$

where $\mathbf{T}_{\nu_s \cdots \nu_1, \alpha_s \cdots \alpha_1}^{(s)} = \langle l_{\nu_s \alpha_s} \cdots l_{\nu_1 \alpha_1} \rangle$ is the average of the transformation tensor where $l_{\nu\alpha}$ is the cosine of the angle between laboratory frame axis $\nu=x, y, z$ and molecular frame axis $\alpha=x, y, z$. The averages of ranks two to five transformation tensors, which are universal quantities independent of system geometry are given in Table I.⁴⁸

Using Table I, the rotational averages of the transition dipoles in Eq. (31) are

$$\langle \mathbf{d}_\xi^{\nu_2} \mathbf{d}_\xi^{\nu_1*} \rangle = \frac{1}{3} \delta_{\nu_2\nu_1} |\mathbf{d}_\xi|^2, \quad (39)$$

$$\langle \bar{\mathbf{d}}_\xi^{\nu_2, \nu_1} \mathbf{d}_\xi^{\nu_1*} \rangle = \frac{1}{6} \epsilon_{\kappa\nu_2\nu_1} \sum_{\alpha_3\alpha_2\alpha_1} \epsilon_{\alpha_3\alpha_2\alpha_1} \bar{\mathbf{d}}_\xi^{\alpha_3, \alpha_2} \mathbf{d}_\xi^{\alpha_1*}. \quad (40)$$

For the averages in Eq. (37) we give only the first two terms

$$\langle \mathbf{d}_{\xi_4}^{\nu_4} \mathbf{d}_{\xi_3}^{\nu_3} \mathbf{d}_{\xi_2}^{\nu_2} \mathbf{d}_{\xi_1}^{\nu_1*} \rangle = \sum_{\alpha_4\alpha_3\alpha_2\alpha_1} \mathbf{T}_{\nu_4\nu_3\nu_2\nu_1, \alpha_4\alpha_3\alpha_2\alpha_1}^{(4)} \mathbf{d}_{\xi_4}^{\alpha_4} \mathbf{d}_{\xi_3}^{\alpha_3} \mathbf{d}_{\xi_2}^{\alpha_2*} \mathbf{d}_{\xi_1}^{\alpha_1*}, \quad (41)$$

$$\langle \bar{\mathbf{d}}_{\xi_4}^{\nu_4, \nu_3} \mathbf{d}_{\xi_3}^{\nu_3} \mathbf{d}_{\xi_2}^{\nu_2*} \mathbf{d}_{\xi_1}^{\nu_1*} \rangle = \sum_{\alpha_5 \cdots \alpha_1} \mathbf{T}_{\nu_4\nu_3\nu_2\nu_1, \alpha_5\alpha_4\alpha_3\alpha_2\alpha_1}^{(5)} \\ \times \bar{\mathbf{d}}_{\xi_4}^{\alpha_5, \alpha_4} \mathbf{d}_{\xi_3}^{\alpha_3} \mathbf{d}_{\xi_2}^{\alpha_2*} \mathbf{d}_{\xi_1}^{\alpha_1*}. \quad (42)$$

The remaining averages differ only by permutation of indices.

Our final expressions, Eqs. (28) and (34) together with Eqs. (31) and (31), allow to calculate all tensor components

of the susceptibilities. The linear susceptibility [Eq. (28)] involves second and third rank rotational averages, while the third-order susceptibility [Eq. (34)] requires fourth and fifth rank averages. Within the dipole approximation we only need second and fourth rank rotational averages involving products of the transition dipoles. Third and fifth rank rotational averages are required when we go beyond the dipole approximation to first order in the wave vector. These averages explicitly include one translational coordinate and, thus, contain qualitatively new information about the molecular geometry. Based on Table I, we find that different ranks in the linear and nonlinear susceptibilities have different symmetry properties: second rank averages in the linear susceptibility are related to a Kronecker δ symbol, while third rank averages are related to a Levi Civita ϵ symbol; these averages and, thus, different orders of the susceptibility in the wave vector can be measured independently with different field configurations. The third-order optical response shows similar trends: the susceptibility in the dipole approximation is related to the fourth rank rotational average, which is proportional to a product of δ functions; to first order in the wave vector the susceptibility is related to the fifth rank rotational average, which contains ϵ . Thus, different orders in the wave vector appear in different tensor components: the dipole approximation gives $xxyy$ and other components with even number of repeating indices, while $xxxy$ and other odd number components only show up beyond the dipole approximation. Each order in the wave vector can thus be measured by a specific configuration of field polarizations.

In general there are 3^4 tensor components in the third order susceptibility, with parametric dependence on both the wave vector direction and amplitude ($|\mathbf{k}_j| = \omega_j/c$, where c is the speed of light). Not all of these components are independent. Table I gives the number of independent tensor components for each order: there is one component in the linear response (related either to δ or ϵ tensor) and three (within the dipole approximation) and six (beyond the dipole approxi-

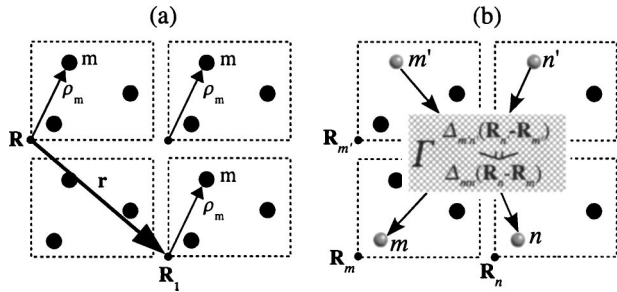


FIG. 2. (Color online) (a) Cells of a periodic infinite system are shown by squares. Each cell has an origin \mathbf{R} and contains several modes (three in the picture are chosen as an example) located at sites m indicated by vectors ρ_m with respect to the cell origin. Each mode is invariant with respect to translation along $\mathbf{r}=\mathbf{R}_1-\mathbf{R}$. (b) Scattering of two excitons in the lattice. Two excitons at sites n' and m' interact with the anharmonic potential Δ [Eq. (E10)] with $\mathbf{r}_2=\mathbf{R}_{n'}-\mathbf{R}_{m'}$ and create another two particles at n and m [Eq. (E11)]. The scattering is translationally invariant in the lattice since the scattering potential depends only on the distance between the cells. Note that momentum before and after scattering is conserved [Eq. (E7)].

mation) components for the third-order response. Additional continuous dependence on the wave vectors constitutes a multidimensional parameter space. For collinear optical fields propagating along z , only x and y polarizations are allowed. This gives three independent tensor elements within the dipole approximation, $xxyy$, $xyxy$, $xyyx$ ($xxxx$ is linearly dependent on these three: from Table I we find that $\langle xxxx \rangle = \langle xxyy \rangle + \langle xyxy \rangle + \langle xyyx \rangle$). Corrections to the dipole approximation induce three new components, $xxxy$, $xyyx$, and $xyxx$.

The rotationally-averaged time-domain expressions when the sequence of interactions is ordered and can be experimentally controlled using short pulses are given in Appendix F.

VI. RESPONSE OF ISOTROPIC ENSEMBLES OF PERIODIC STRUCTURES

We consider a periodic \mathcal{D} dimensional lattice made of $N^{\mathcal{D}}$ cells with \mathcal{M} sites (modes) per unit cell, a lattice constant a and volume $\mathcal{V}=(Na)^{\mathcal{D}}$ as shown in Fig. 2. The position of the m th site is given by the vector $\mathbf{R}+\rho_m$, where \mathbf{R} is the origin of the unit cell and ρ_m is the displacement from that origin.

The exciton Bloch states are described by two quantum numbers: \mathbf{q} is the exciton momentum within the band and λ is the Davydov subband. In general there are $N^{\mathcal{D}}$ values of momenta and \mathcal{M} Davydov subbands. The Bloch states and Green's functions for a periodic system are given in Appendix D. Expanding the linear and the third-order susceptibilities in eigenstates we obtain general expressions for the linear and the third-order susceptibilities [Eqs. (D5) and (D7)].

For small periodic systems (when $N \gg 1$ but $L=Na \ll |\mathbf{k}|^{-1}$) we can use the expansion in wave vectors. Using the Bloch eigenstates in Eqs. (28) and (34) and performing rotational averagings [Eqs. (31) and (37)] we find that only zero momenta contribute to the optical response and obtain

$$\begin{aligned} \chi_{\nu_2, \nu_1}^{(1)}(-\mathbf{k}_2 - \omega_2; \mathbf{k}_1 \omega_1) &= 2\pi i \mathcal{V} \delta(\omega_2 - \omega_1) \\ &\times \sum_{\lambda} \langle \mathbf{M}_{\lambda\lambda}^{\nu_2, \nu_1}(\mathbf{k}_2, \mathbf{k}_1) \rangle I_{\lambda}(\omega_2) \\ &+ \text{c. c.}', \end{aligned} \quad (43)$$

where the prime now indicates a summation over different Davydov's subbands (whose number is equal to the number of sites in the unit cell), \mathcal{V} is the volume of the molecule and

$$\begin{aligned} \langle \mathbf{M}_{\lambda\lambda}^{\nu_2, \nu_1}(\mathbf{k}_2, \mathbf{k}_1) \rangle &= \langle d_{\lambda}^{\nu_2} d_{\lambda}^{\nu_1} \rangle + i \sum_{\kappa} \mathbf{k}_2^{\kappa} \langle \bar{d}_{\lambda}^{\kappa, \nu_2} d_{\lambda}^{\nu_1} \rangle \\ &- \mathbf{k}_1^{\kappa} \langle \bar{d}_{\lambda}^{\kappa, \nu_2} d_{\lambda}^{\nu_1} \rangle. \end{aligned} \quad (44)$$

For the nonlinear susceptibility we similarly obtain

$$\begin{aligned} \chi_{\nu_4, \nu_3, \nu_2, \nu_1}^{(3)}(-\mathbf{k}_4 - \omega_4; \mathbf{k}_3 \omega_3, \mathbf{k}_2 \omega_2, \mathbf{k}_1 \omega_1) &= 2\pi i \mathcal{V}^2 \delta(\omega_4 - \omega_3 - \omega_2 - \omega_1) \mathcal{P}_{\nu\kappa\omega} \\ &\times \sum_{\lambda_4 \dots \lambda_1} \langle \mathbf{M}_{\lambda_4 \lambda_3 \lambda_2 \lambda_1}^{\nu_4 \nu_3 \nu_2 \nu_1}(\mathbf{k}_4 \mathbf{k}_3 \mathbf{k}_2 \mathbf{k}_1) \rangle \Gamma_{\lambda_4 \lambda_3 \lambda_2 \lambda_1}(\omega_2 + \omega_1) \\ &\times I_{\lambda_4}(\omega_4) I_{\lambda_3}^*(-\omega_3) I_{\lambda_2}(\omega_2) I_{\lambda_1}(\omega_1) + \text{c. c.}' \end{aligned} \quad (45)$$

with the orientational tensors

$$\begin{aligned} \langle \mathbf{M}_{\lambda_4 \lambda_3 \lambda_2 \lambda_1}^{\nu_4 \nu_3 \nu_2 \nu_1}(\mathbf{k}_4 \mathbf{k}_3 \mathbf{k}_2 \mathbf{k}_1) \rangle &= \langle d_{\lambda_4}^{\nu_4} d_{\lambda_3}^{\nu_3} d_{\lambda_2}^{\nu_2} d_{\lambda_1}^{\nu_1} \rangle \\ &+ i \sum_{\kappa} \mathbf{k}_4^{\kappa} \langle \bar{d}_{\lambda_4}^{\kappa, \nu_4} d_{\lambda_4}^{\nu_3} d_{\lambda_3}^{\nu_2} d_{\lambda_1}^{\nu_1} \rangle \\ &- i \sum_{\kappa} \mathbf{k}_3^{\kappa} \langle \bar{d}_{\lambda_3}^{\kappa, \nu_3} d_{\lambda_4}^{\nu_3} d_{\lambda_2}^{\nu_2} d_{\lambda_1}^{\nu_1} \rangle \\ &- i \sum_{\kappa} \mathbf{k}_2^{\kappa} \langle \bar{d}_{\lambda_2}^{\kappa, \nu_2} d_{\lambda_3}^{\nu_2} d_{\lambda_3}^{\nu_3} d_{\lambda_4}^{\nu_4} d_{\lambda_1}^{\nu_1} \rangle \\ &- i \sum_{\kappa} \mathbf{k}_1^{\kappa} \langle \bar{d}_{\lambda_1}^{\kappa, \nu_1} d_{\lambda_3}^{\nu_3} d_{\lambda_2}^{\nu_2} d_{\lambda_4}^{\nu_4} \rangle. \end{aligned} \quad (46)$$

The one-exciton Green's functions [Eq. (D4)] and the scattering matrix [Eq. (E12)] are taken at $\mathbf{q}=0$. κ and ν are cartesian components of the field wave vector and polarization, respectively, and the rotational averages may be calculated using Eqs. (39)–(42).

VII. APPLICATION TO HELICAL POLYPEPTIDES

We have calculated the nonlinear susceptibility of the amide I vibrational mode of α and 3_{10} helical polypeptides. The helical periodic structures were created by repeating the operations of translation along the helix axis z and rotation of the xy plane around that z axis by placing each peptide residue for both systems according to Table II. The resulting 2.5 nm (0.5 nm) one-dimensional unit cell has 18 (3) residues for α (3_{10}) helix. The parameters for the transition dipole orientations and for the couplings between neighboring modes were taken from our previous work⁷⁰ with the diagonal anharmonicity $V_{mm,mm} = 2U_{mm,mm} \equiv \Delta = -16 \text{ cm}^{-1}$.

We constructed a momentum space Hamiltonian for the infinite systems [Eq. (D2)] and calculated the one-exciton eigenstates. The susceptibilities were calculated using Eqs. (43) and (45) with the rotational averages obtained from Eqs. (39)–(42). The Green's functions in the exciton basis were

TABLE II. Parameters of α and 3_{10} helices for transition dipoles.

	α helix	3_{10} helix
Translation distance along z (nm)	0.138	0.183
Rotation angle around z (deg)	100	120
Initial transition dipole ^a	(-0.271, -0.309, 0.912)	(-0.453, -0.325, 0.830)
Initial coordinate of the transition dipole (nm)	(1.76, 0, 0)	(1.42, 0, 0)
Number of sites in the unit cell	18	3

^aThe transition dipole is normalized so that the amplitude is 1.

calculated using Eq. (D4). Uniform line broadening $\gamma_\lambda(\mathbf{q}) = 3 \text{ cm}^{-1}$ was assumed for all one-exciton states. The scattering matrix was calculated using Eqs. (E8)–(E12). A grid of $N=100$ momenta was used to evaluate the integral in Eq. (E9). The relevant energy levels form three well-separated manifolds of states as shown in Fig. 5(a): the ground state, the one-exciton, and the two-exciton manifold. The bandwidths of these manifolds (determined by J and Δ) are much smaller than the energy gaps between them.

The absorption lineshapes of linearly polarized light of both helices calculated using Eq. (22) are presented in Fig. 3. Both spectra show two peaks resulting from three (one longitudinal and two degenerate transverse) transitions.⁷⁰ The corresponding frequencies are 1642 and 1661 cm^{-1} for the α helix and 1646 and 1677 cm^{-1} for the 3_{10} helix. The transverse peaks are relatively weaker for the α helix. The CD spectrum calculated using Eq. (23) has also a two peak structure corresponding to the two peaks in linear absorption. Both peaks have equal amplitudes but different signs: the longitudinal peak is positive and the transverse is negative.

Linear spectroscopy shows only transitions between the ground state and the one-exciton states. Qualitatively new information is contained in third-order spectroscopy. We have calculated the CW signal for a collinear configuration assuming that all fields propagate along z . Taking into account the dispersion relation between wave vector amplitudes and the frequencies, the susceptibility becomes a function of three variables ($\omega_1, \omega_2, \omega_3$) with three independent tensor elements, $xxyy$, $xyyx$, and $xyxy$, in the dipole approxi-

mation and three additional elements, $xxxy$, $xyyx$, and $xyxx$, beyond that approximation. We calculated the signal observed in the direction $\mathbf{k}_1 + \mathbf{k}_2 - \mathbf{k}_3$ with $\omega_3 = -\omega_1$.

The tensor components $xxyy$ and $xyyx$ of α helix shown in Fig. 4 originate from the dipole approximation ($xyyx$ is very similar to $xxyy$ and is not shown). They show one strong (longitudinal) diagonal peak at $\omega_1 = \omega_2 = 1642 \text{ cm}^{-1}$ and a weak (transverse) peak at $\omega_1 = \omega_2 = 1661 \text{ cm}^{-1}$ in α helix. The weak crosspeaks between these diagonal peaks are best seen in $xyyx$.

The chirally-sensitive susceptibilities calculated beyond the dipole approximation ($xxxy$ and $xyyx$ in Fig. 4) show a similar pattern. The largest difference is in the crosspeaks: they are very asymmetric with respect to the diagonal line and one of them has an amplitude comparable to the strongest diagonal peak.

The corresponding 3_{10} spectra are also shown. The longitudinal diagonal peak shows at $\omega_1 = \omega_2 = 1647 \text{ cm}^{-1}$ and the weaker transverse at $\omega_1 = \omega_2 = 1677 \text{ cm}^{-1}$. Since both systems are right-handed helices the information contained is similar: the 3_{10} helix shows larger separation between the peaks and stronger crosspeaks compared to the α helix. The crosspeaks are symmetric with respect to diagonal ($\omega_1 = \omega_2$) in the dipole approximation. The corresponding crosspeaks have different amplitudes beyond that approximation.

Our simulated peak positions correlate well with experiments^{26,71–73} and previous calculations.^{74–76} They show that the crosspeaks carry information about exciton interactions and distances between them: new terms such as $xxxy$ give an asymmetric crosspeak pattern, with comparable amplitudes to the diagonal peaks. This signal also has a complicated dependence on coordinates and should vanish for achiral systems. However, only one-exciton resonances are seen in this signal. The four one-exciton Green's functions suppress the two exciton resonances contained in the scattering matrix [see Eq. (45)].

We next consider techniques that reveal two-exciton resonances. We start with the following 2D $\mathbf{k}_1 + \mathbf{k}_2 - \mathbf{k}_3$ signal:

$$W_{\nu_4 \nu_3 \nu_2 \nu_1}(\omega_3, \omega) \equiv \int d\omega' \chi_{\nu_4, \nu_3 \nu_2 \nu_1}^{(3)}(\omega_3 - \omega; -\omega_3, \omega/2 + \omega', \omega/2 - \omega') \quad (47)$$

with the optical frequencies tuned according to Fig. 5(b) where both $\omega/2$ and ω_3 are tuned to the one-exciton resonances (ω also covers two-exciton resonances), while ω' is

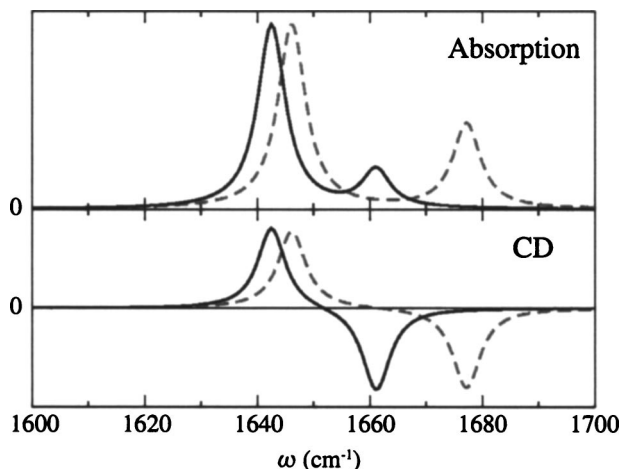


FIG. 3. (Color online) Linear absorption (top) and circular dichroism (bottom) spectra of the infinite α (black solid) and 3_{10} (red dashed) helices in the amide I region (spectra are normalized so that the largest peaks are equally strong).

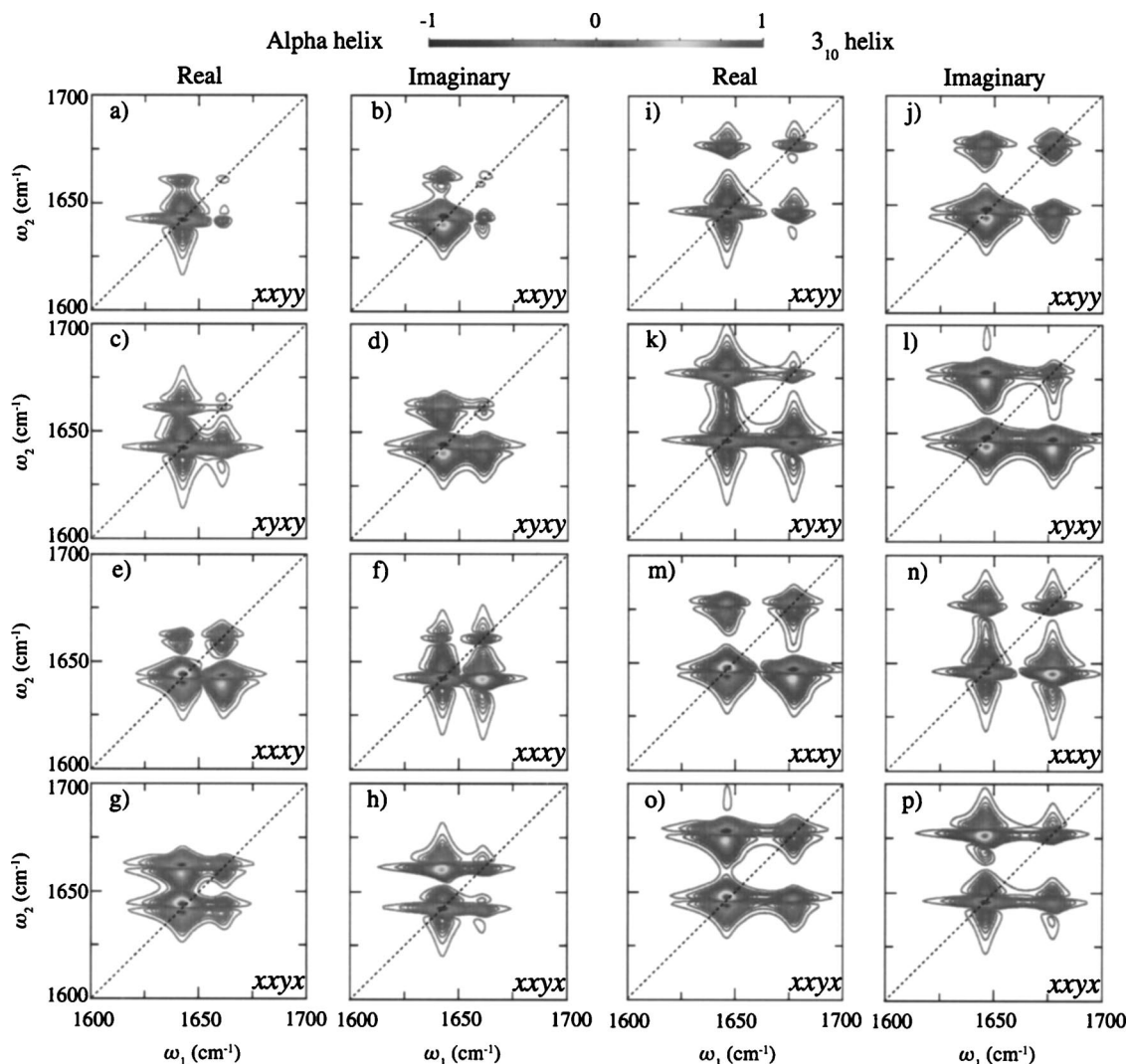


FIG. 4. Third-order susceptibility tensor, $\chi_{\nu_4\nu_3\nu_2\nu_1}(-\omega_2; -\omega_1, \omega_2, \omega_1)$, of α helix (two left columns) and of 3_{10} helix (two right columns) as a function of ω_1 and ω_2 . Both real and imaginary parts are shown. Two tensor elements χ_{xxxxy} and χ_{xyxy} are calculated in the dipole approximation. The chirally sensitive tensor elements χ_{xxxxy} and χ_{xyxy} vanish in the dipole approximation.

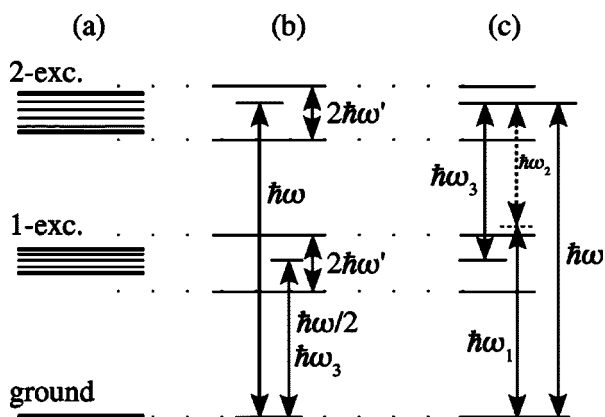


FIG. 5. (a) Energy level scheme of coupled amide I vibrations. The ground, one-exciton, and two-exciton manifolds are shown for the amide I band. The band widths of the one-exciton and two-exciton manifolds are roughly 50 and 100 cm^{-1} , respectively. The energy gaps between them are 1600 cm^{-1} . Two experimental configurations are shown: (b) all fields are resonant with excitonic transitions; (c) ω_1 and ω_2 are nonresonant, but $\omega = \omega_1 + \omega_2$ is resonant.

much smaller than the one-exciton energy as shown in Fig. 5(b). The resonant terms in the susceptibility for this configuration are of the form $\Gamma_{\lambda_4\lambda_3\lambda_2\lambda_1}(\omega) \times I_{\lambda_4}(\omega - \omega_3) I_{\lambda_3}^*(-\omega_3) I_{\lambda_2}(\omega/2 + \omega') I_{\lambda_1}(\omega/2 - \omega')$. The signal has the frequency $\omega_3 - \omega$ and in the dipole approximation becomes

$$W_{\nu_4\nu_3\nu_2\nu_1}^{(dip)}(\omega_3, \omega) \propto i \sum'_{\lambda_4 \dots \lambda_1} \langle d_{\lambda_4}^{\nu_4} d_{\lambda_3}^{\nu_3} d_{\lambda_2}^{\nu_2} d_{\lambda_1}^{\nu_1} \rangle I_{\lambda_4}(\omega - \omega_3) \times I_{\lambda_3}^*(\omega_3) \Gamma_{\lambda_4\lambda_3\lambda_2\lambda_1}(\omega) \mathcal{I}_{\lambda_2\lambda_1}(\omega). \quad (48)$$

This signal involves the product $\Gamma_{\lambda_4\lambda_3\lambda_2\lambda_1}(\omega) \mathcal{I}_{\lambda_2\lambda_1}(\omega)$ which is the two-exciton Green's function in the exciton basis [see Eq. (A15)], showing two-exciton resonances along the ω axis. By integrating the signal over ω_3

$$\bar{W}_{\nu_4\nu_3\nu_2\nu_1}(\omega) \equiv \int d\omega_3 W_{\nu_4\nu_3\nu_2\nu_1}(\omega_3, \omega), \quad (49)$$

we obtain in the dipole approximation

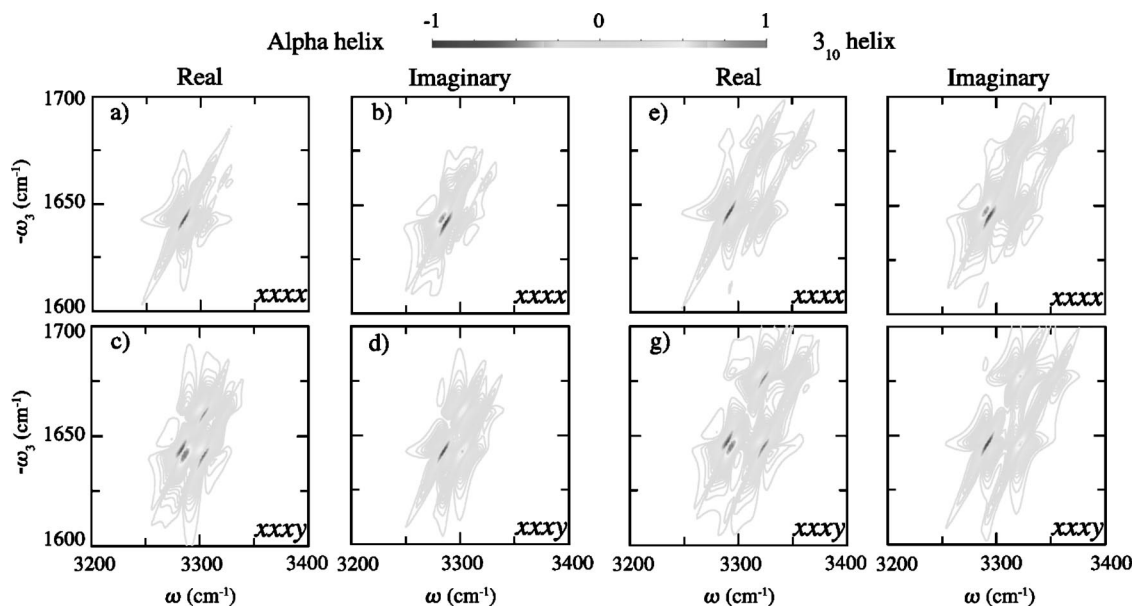


FIG. 6. Third-order signal $W_{\nu_4\nu_3\nu_2\nu_1}(\omega_3, \omega)$ [Eq. (47)] of α helix (two left columns) and of 3_{10} helix (two right columns). W_{xxxx} (dipole approximation) and W_{xxyy} (chirally sensitive) are shown.

$$\begin{aligned} \overline{W}_{\nu_4\nu_3\nu_2\nu_1}^{(dip)}(\omega) &\equiv \int d\omega_3 W_{\nu_4\nu_3\nu_2\nu_1}^{(dip)}(\omega_3, \omega) \\ &\propto i \sum'_{\lambda_4 \dots \lambda_1} \langle d_{\lambda_4}^{\nu_4} d_{\lambda_3}^{\nu_3} d_{\lambda_2}^{\nu_2} d_{\lambda_1}^{\nu_1} \rangle \Gamma_{\lambda_4\lambda_3\lambda_2\lambda_1}(\omega) \mathcal{I}_{\lambda_2\lambda_1}(\omega), \end{aligned} \quad (50)$$

$$\begin{aligned} \overline{U}_{\nu_4\nu_3\nu_2\nu_1}^{(dip)}(\omega) &\equiv \int d\omega_3 U_{\nu_4\nu_3\nu_2\nu_1}^{(dip)}(\omega_3, \omega) \\ &\propto \frac{1}{\omega_1 - \overline{\Omega}} \sum'_{\lambda_4 \dots \lambda_1} \langle d_{\lambda_4} d_{\lambda_3} d_{\lambda_2} d_{\lambda_1} \rangle \Gamma_{\lambda_4\lambda_3\lambda_2\lambda_1}(\omega). \end{aligned} \quad (53)$$

which only shows two-exciton resonances.

A different experiment can be performed by detuning ω_1 and ω_2 off resonance ($\omega_1 - \overline{\Omega} > \overline{\gamma}$), but $\omega_2 + \omega_1 = \omega \approx 2\overline{\Omega}$ covers the two-exciton band (here $\overline{\Omega}$ is the average one-exciton excitation energy and $\overline{\gamma}$ is the average dephasing) [see Fig. 5(c)]. Again the contribution to this signal comes from terms such as $\Gamma_{\lambda_4\lambda_3\lambda_2\lambda_1}(\omega) I_{\lambda_4}(\omega - \omega_3) I_{\lambda_3}^*(\omega_3) I_{\lambda_2}(\omega - \omega_1) I_{\lambda_1}(\omega_1)$, where ω_1 is fixed. Taking into account that $I_{\lambda_1}(\omega_1)$ is constant and $I_{\lambda_2}(\omega - \omega_1)$ is not resonant ($|\omega - \omega_1 - \overline{\Omega}| \gg \overline{\gamma}$) we define the signal

$$\begin{aligned} U_{\nu_4\nu_3\nu_2\nu_1}(\omega_3, \omega) &\equiv (\omega - \omega_1 - \overline{\Omega}) \\ &\quad \times \chi_{\nu_4\nu_3\nu_2\nu_1}^{(3)}(\omega_3 - \omega, -\omega_3, \omega - \omega_1, \omega_1), \end{aligned} \quad (51)$$

where the factor $(\omega - \omega_1 - \overline{\Omega})$ is included to approximately compensate the asymmetry of by $I_{\lambda_2}(\omega - \omega_1)$. By integration over ω_3 we have

$$\overline{U}_{\nu_4\nu_3\nu_2\nu_1}(\omega) \equiv \int d\omega_3 U_{\nu_4\nu_3\nu_2\nu_1}(\omega_3, \omega). \quad (52)$$

In the dipole approximation we obtain

This signal is proportional to the scattering matrix and is scaled by $(\omega_1 - \overline{\Omega})^{-1}$, which is an average off-resonant detuning. Thus, both the \overline{W} and \overline{U} signals carry information on two-exciton resonances: the former shows the two-exciton Green's function, the latter shows the two-exciton scattering matrix. The \overline{W} signal is resonant and should be stronger than \overline{U} .

Going beyond the dipole approximation, the rotational factors depend on the wave vectors and, thus, optical frequencies and the integrations do not lead to such simple expressions. However, the resonances should still reflect the two-exciton states, with different amplitudes and lineshapes.

$W_{\nu_4\nu_3\nu_2\nu_1}(\omega_3, \omega)$ displayed in Fig. 6 shows two-exciton mixed with one-exciton resonances. The chirally-sensitive components show peaks at the same positions as in the dipole approximation, but different relative amplitudes. This is a consequence of the fact that the molecular Hamiltonian is not affected by the dipole approximation, thus, the resonances remain the same. However, peak amplitudes, controlled by rotational factors are different.

$\overline{W}_{\nu_4\nu_3\nu_2\nu_1}(\omega)$ for the helices displayed in Fig. 7 show three two-exciton resonances which are better resolved in the 3_{10} helix compared to the α helix. The amplitudes of two-exciton resonances show dramatic differences when going beyond the dipole approximation: the central resonance becomes stronger. This effect is more pronounced for 3_{10} helix compared to α helix.

The $U_{\nu_4\nu_3\nu_2\nu_1}(\omega_3, \omega)$ signals displayed in Fig. 8 show one-exciton resonances superimposed with two-exciton reso-

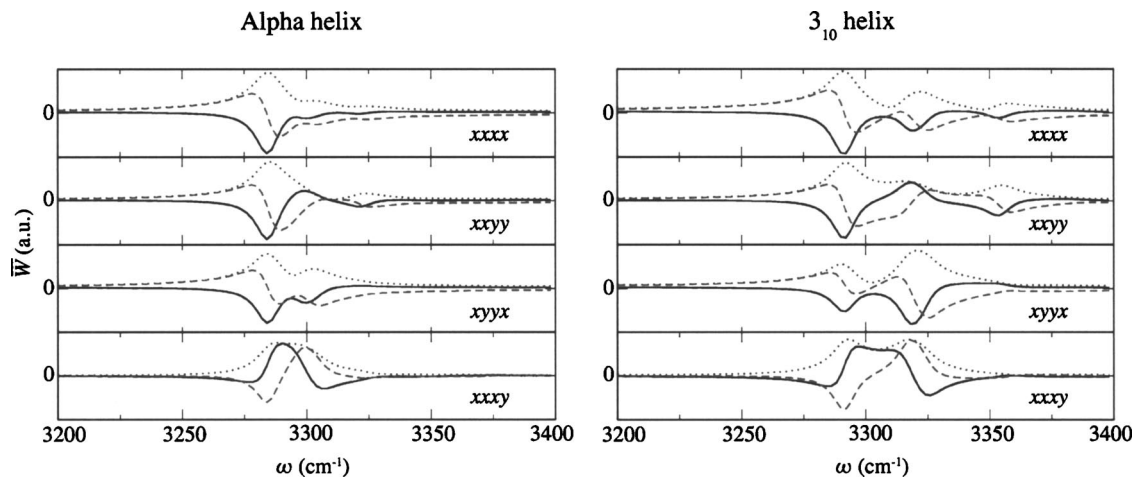


FIG. 7. (Color online) Third-order signal $\overline{W}_{\nu_4\nu_3\nu_2\nu_1}(\omega)$ [Eq. (49)] of α helix (left) and of 3_{10} helix (right). Four tensor elements are shown: \overline{W}_{xxxx} , \overline{W}_{xyyy} , \overline{W}_{xyyx} (all three in the dipole approximation), and \overline{W}_{xxyy} (chirally sensitive). Solid-real, dashed-imaginary, dotted-absolute value.

nances. These signals decay very slowly with off-resonance detuning. Thus, measuring the susceptibility over a broad frequency range is required to get this signal, as is clearly seen for U displayed in Fig. 9. These figures demonstrate the scattering matrix weighted by the orientational factors and show a complicated picture of two exciton resonances: one part of the signal (real in the dipole approximation and imaginary beyond it) has a background plateau, whose magnitude is related to the anharmonicity. This can be easily shown by considering the scattering matrix of a single anharmonic vibrational mode. The different distribution of the amplitudes in the α and the 3_{10} helices is much more clearly seen in these two-exciton related signals compared with the one-exciton spectra shown in Fig. 4.

VIII. DISCUSSION

The linear absorption is described by the electric dipole approximation which is related to the diagonal tensor ele-

ments of the linear susceptibility. CD spectroscopy is related to the off-diagonal tensor elements, which vanish for isotropic systems in the electric dipole approximation. The CD signal is induced by the magnetic dipole or higher electric multipoles. The magnetic transition dipoles may be neglected for extended systems e.g., macromolecules, as will be shown below.

We considered a model systems of coupled electric dipoles distributed in space. The calculations done for helices can be repeated to other secondary structure motifs such as β sheets and random coils, and to electronic aggregates. Going beyond the dipole approximation, which is equivalent to including the positions of the dipoles, is required for CD. The nonlocal susceptibilities were expanded to first order in the wave vectors: the expansion of molecular property functions in wave vector accounts for higher multipoles.

The wave vector expansion requires additional condi-

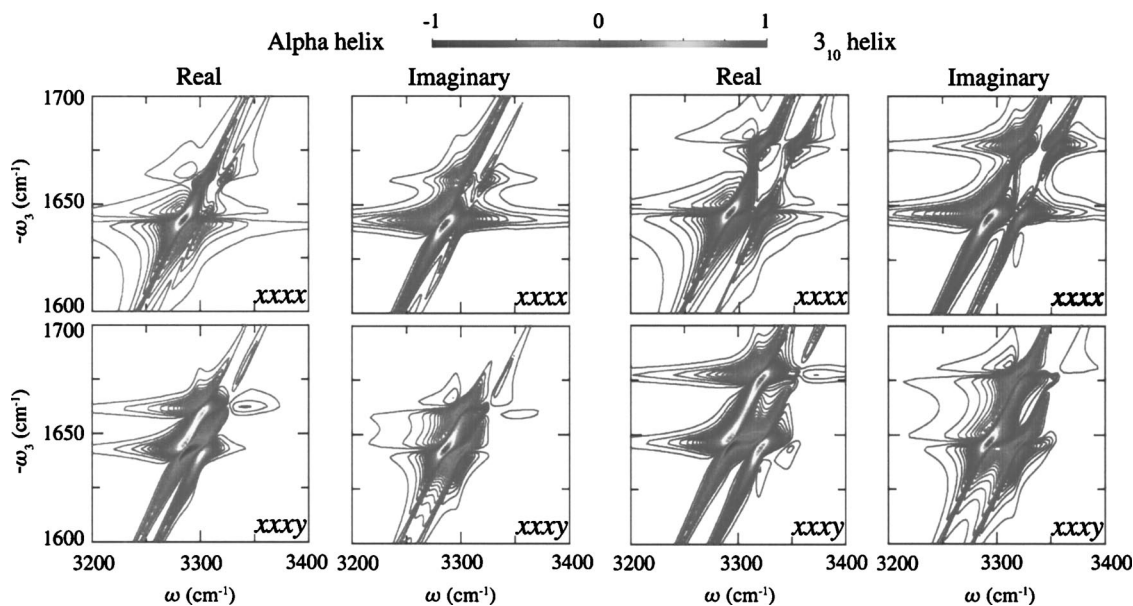


FIG. 8. Third-order signal $U_{\nu_4\nu_3\nu_2\nu_1}(\omega_3, \omega)$ [Eq. (51)] of α helix (two left columns) and of 3_{10} helix (two right columns). U_{xxxx} (dipole approximation) U_{xxyy} (chirally sensitive) are shown. $\omega_1=1800 \text{ cm}^{-1}$ and $\Omega=1650 \text{ cm}^{-1}$.

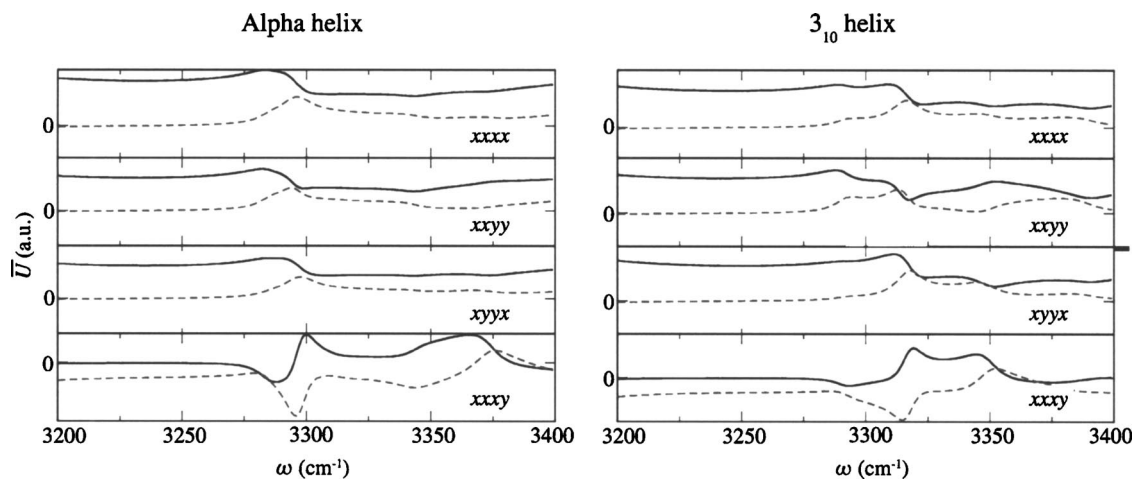


FIG. 9. (Color online) Third-order signal $\bar{U}_{\nu_4\nu_3\nu_2\nu_1}(\omega)$ [Eq. (52)] of α helix (left) and of 3_{10} helix (right). Four tensor elements are shown: \bar{U}_{xxxx} , \bar{U}_{xyxy} , \bar{U}_{xyyx} (all three in the dipole approximation), and \bar{U}_{xxxy} (chirally sensitive). Solid-real; dashed-imaginary. Parameters are the same as in Fig. 8

tions. The system size L is limited from above by $\mathbf{k}_0 L \ll 1$, where \mathbf{k}_0 is an optical wave vector. For larger systems L must be replaced by the exciton coherence size.⁷⁷ The limit, thus, holds even for large molecular systems including proteins and electronic aggregates. The system size is also limited from below since the magnetic transition dipoles may not be neglected for small systems. The expansion $\exp(i\mathbf{k}\mathbf{r}) \approx 1 + i\mathbf{k}\mathbf{r}$ suggests that the amplitude of the terms linear in \mathbf{k} are $L|\mathbf{k}|$. The local magnetic transition dipoles are proportional to the factor v/c ,⁴⁰ where v is the speed of electron for electronic transitions or the speed of nuclei for vibrational transitions and c is the speed of light. Thus, $L > v/\omega$; ω is the optical frequency. This ratio can be estimated by assuming classical energy: $mv^2 = 2\hbar\omega$, where m is the mass of particle and $\hbar\omega$ is its energy. We can then express this limit as $L > \sqrt{2\hbar/m\omega}$. For instance, taking values of hydrogen atom with excitation energy corresponding to 3000 cm^{-1} we obtain $L > 0.1 \text{ nm}$ for vibrational transitions. Thus, our approach holds for delocalized excitons with coherence size spanning several units.

Periodicity reduces the problem size considerably: the necessary sums reduce from the total number of dipoles to the number of modes in a unit cell (for linear J aggregates⁷⁸ it is just one site). We have derived the response function and the susceptibility for infinite systems. This seems to conflict with the upper bound of the system size. However, the system can be assumed infinite as long as the number of cells is very large, $N \gg 1$, and edge effects can be ignored. We performed calculations on amide I transitions of infinite helical peptide. Since the distance between residues is $\sim 0.5 \text{ nm}$, our

approach is valid when the coherence size of excitation is larger than two residues, which is reasonable at ambient temperatures. Several hundreds of residues are required to reach the 100 nm length of the α helical structure, which validates the infinite size assumption. Even when the physical size of the system is larger than the wavelength, the exciton coherence size is typically smaller than the wavelength; this limit is always satisfied for vibrational transitions of polypeptides.

Second-order techniques for probing molecular chirality are commonly used for isotropic systems. Second harmonic generation (SHG) is not allowed in the dipole approximation by symmetry.^{79,80} For this reason most studies of quadratic nonlinearities were conducted on macroscopically noncentrosymmetric systems.^{81,82} However, sum frequency generation (SFG) of isotropic systems in a noncollinear configuration is allowed and is used as a probe of molecular chirality.^{83–86} Symmetry of isotropic systems allows one specific, xyz , component of the second-order susceptibility tensor to be finite in the dipole approximation. Noncollinear configuration leads to breaking of phase-matching condition and, thus, to weak signals.^{84,85,87} Even weaker SHG signal was observed, showing the significance of magnetic transition dipoles and of electronic quadrupoles. However this SHG signal originating from terms beyond the dipole approximation is not sensitive to molecular chirality.

We next consider the symmetry properties of rotational averages shown in Table III with respect to different spectroscopies and chirality. Only one independent diagonal tensor component, xx , of the linear response survives the isotropic rotational averaging in the dipole approximation; all off

TABLE III. Symmetry properties of rotational averages with respect to chirality tensor.

Response	Form of terms in isotropic averaging	Independent nonzero elements	Probe of chirality?
1st (dipole)	$\delta_{\nu_2\nu_1}$	xx	n
1st ($i\mathbf{k}\mathbf{r}$ related)	$\epsilon_{\kappa\nu_2\nu_1}$	$(z)yx$	y
2nd (dipole)	$\epsilon_{\nu_3\nu_2\nu_1}$	xyz	y
2nd ($i\mathbf{k}\mathbf{r}$ related)	$\delta_{\kappa\nu_3}\delta_{\nu_2\nu_1}$	$(x)xyy, (x)yxyx, (x)yxxy$	n
3rd (dipole)	$\delta_{\nu_4\nu_3}\delta_{\nu_2\nu_1}$	$xyxy, xyyx, xyxy$	n
3rd ($i\mathbf{k}\mathbf{r}$ related)	$\delta_{\nu_4\nu_3}\epsilon_{\kappa\nu_2\nu_1}$	$(z)xxxy, (z)xyxy, (z)xyyx, (z)zxyz, (z)zxzy, (z)zzyx$	y

diagonal components (and consequently the CD signal) vanish. Calculating the linear response to first order in wave vector, requires a third rank rotational averaging involving the positions of the dipoles. The tensor is then proportional to $\epsilon_{\kappa\nu_2\nu_1}$ —a Levi-Civita permutation symbol.⁴⁸ Thus, one independent, xyz , component is nonzero, relating the propagation direction (for instance, z) and polarization (x and y) of the optical field and system polarization.

The number of scalar products to be averaged is intimately related to the chirality of the system. An achiral system can be superimposed on itself after spatial inversion parity operation,¹ thus, the rotational average needs to be the same for the original and the inverted systems. Odd rank rotational averages which change sign upon inversion must therefore vanish. A chiral system, in contrast, is converted to its mirror image by parity operation and the two cannot be superimposed, thus, odd rank rotational averages are nonzero and carry opposite signs for enantiomers. Therefore only chiral systems survive odd rank rotational averagings. Even rank rotational averages are not sensitive to spatial inversion and, therefore, to chirality. Thus, the tensors involving odd rank rotational averages are chirally-sensitive.

Third rank rotational averaging is responsible for the second-order response in the dipole approximation. The isotropic average is then proportional to the Levi-Civita tensor leading to xyz tensor element of second-order susceptibility. This element is not accessible by the collinear configuration, required for phase matching. Similar to CD, this rotational average survives only for isotropic systems with chiral molecules. Going one step beyond the dipole approximation we obtain a chirally insensitive signal coming from fourth rank rotational averaging.⁷⁹

The third-order nonlinear response in the dipole approximation has three independent nonzero rotational averages, $xyxy$, $xyyx$ and $xyxy$; the signal is not chirally sensitive. Going beyond the dipole approximation leads to the fifth rank orientational averaging which imposes dependence of the signal on the field wave vectors and includes the positions of the dipoles. Fifth rank averaging gives six independent nonzero tensor elements: $zxxx$, $zxyx$, $zxyxx$, $zxyyz$, $zxyz$, and $zzyxy$ which participate in noncollinear configurations. These elements now carry information about chirality for the same reasons as xyz in circular dichroism.

Phase-matching in the third-order response defines the signal propagation direction. Unlike SFG, the collinear configuration, which gives the strongest signal is allowed in the third-order response and has three independent tensor elements: $(z)xxx$, $(z)xyyx$, and $(z)xyxx$ (fields propagate along z). The frequency permutation requirement in the susceptibility implies that they all vanish when $\omega_1 = \omega_2 = \omega_3$ (i.e., third harmonic generation). Noncollinear configuration (which can also satisfy phase matching) leads to six nonzero rotational averages where all components participate in the response. Thus, the third-order response beyond the dipole approximation together with CD constitute the best probes of chirality and carry more information than conventional linear and third-order response within the dipole approximation and SFG.

We have derived expressions for the response using the

NEE, which are based on a standard exciton Hamiltonian in the Heitler-London approximation. The parameters of this Hamiltonian are excitation energies of different modes, intermode couplings (quadratic), and anharmonicities (quartic couplings), as well as excitation transition dipole and its coordinate. These parameters may be obtained from *ab initio* calculations performed on small peptide segments.^{74,88,89} They can also be readily obtained from experiment. The excitation energies and intermode couplings are observed in linear absorption and CD. We assumed only local anharmonicities, which give a shift of one double excitation energy from twice the single excitation energy on the same mode. This can be obtained from pump-probe measurements. Off-diagonal anharmonicities may also be important when intermode coupling is weak.⁶⁰

The experimental techniques which show two-exciton resonances are most promising since they carry qualitatively new information about the system. They also show very strong dependence on the structure of the peptide backbone. The tensor components induced by deviations from the dipole approximation show strong differences between the two helices. Compared to CD, different exciton states are probed, the signal originates from the anharmonicity and multiple transition dipoles with the coordinates define the signal. The frequency integrated susceptibilities used in our definitions of the U and W signals [Eqs. (47) and (51)] could be obtained in time-domain experiments using short optical pulses which have a broad spectral bandwidth.

ACKNOWLEDGMENTS

This material is based upon work supported by the National Science Foundation Grant No. CHE-0132571. The support of the National Institutes of Health Grant No. 1 RO1 GM59230-10A2 was gratefully acknowledged.

APPENDIX A: EXCITON BASIS SET, GREEN'S FUNCTIONS, AND THE SCATTERING MATRIX

The eigenenergies Ω_ξ and eigenvectors $\psi_{\xi m}$ of the one-exciton block of the Hamiltonian [Eq. (2)], $\langle 0\hat{B}_m|\hat{H}|\hat{B}_n^\dagger 0\rangle \equiv h_{m,n} = \delta_{m,n}\epsilon_m + J_{m,n}(1 - \delta_{m,n})$, define the one-exciton basis,

$$\sum_n h_{m,n}\psi_{\xi n} = \Omega_\xi\psi_{\xi m}. \quad (\text{A1})$$

The evolution of a single exciton following an impulsive excitation is described by the one-exciton Green's function $G(t)$,

$$B_m(t) = \sum_{m'} G_{m,m'}(t)B_{m'}(0), \quad (\text{A2})$$

which satisfies the equation

$$\frac{dG_{m,n}(t)}{dt} + i\sum_{n'} h_{m,n'}G_{n',n}(t) = \delta(t). \quad (\text{A3})$$

This equation can be solved using the exciton eigenvalues $\psi_{\xi m}$. The one-exciton Green's function is then given by

$$G_{m,n}(t) = \sum_{\xi} \psi_{\xi m} I_{\xi}(t) \psi_{\xi n}^*, \quad (\text{A4})$$

where

$$I_{\xi}(t) = \theta(t) \exp(-i\Omega_{\xi}t - \gamma_{\xi}t) \quad (\text{A5})$$

is a Green's function in the eigenstate basis, γ_{ξ} is a dephasing rate, and $\theta(t)$ is the step function [$\theta(t)=0$ for $t<0$ and $\theta(t)=1$ for $t\geq 0$] which guarantees causality.

Applying the Fourier transform [Eq. (9)] to Eqs. (A4) and (A5) we obtain the frequency domain Green's function,

$$G_{m,n}(\omega) = \sum_{\xi} \psi_{\xi m} I_{\xi}(\omega) \psi_{\xi n}^* \quad (\text{A6})$$

with

$$I_{\xi}(\omega) = \frac{i}{\omega - \Omega_{\xi} + i\gamma_{\xi}}. \quad (\text{A7})$$

The two-exciton evolution $Y_{mn}(t)$ is similarly described by the two-exciton Green's function \mathcal{G}^Y

$$Y_{mn}(t) = \sum_{m'n'} \mathcal{G}_{mn,m'n'}^Y(t) Y_{m'n'}(0), \quad (\text{A8})$$

which satisfies the equation

$$\frac{d\mathcal{G}_{mn,m'n'}^Y}{dt} + i \sum_{m''n''} (h_{mn,m''n''}^{(Y)} + V_{mn,m''n''}) \mathcal{G}_{m''n'',m'n'}^Y = \delta(t). \quad (\text{A9})$$

The zero-order noninteracting ($V=0$) two-exciton Green's function \mathcal{G} can be factorized into a product of one-exciton Green's functions, $\mathcal{G}_{mn,m'n'}(t) = G_{m,m'}(t)G_{n,n'}(t)$. The actual Green's function, \mathcal{G}^Y , is connected to \mathcal{G} by the Bethe Salpeter equation

$$\mathcal{G}^Y(t) = \mathcal{G}(t) + \int_0^t dt' \int_0^{t'} dt_1 \mathcal{G}(t-t') \Gamma(t'-t_1) \mathcal{G}(t_1), \quad (\text{A10})$$

where we have introduced the two exciton scattering matrix $\Gamma(t'-t_1)$. The two-exciton Green's function and the scattering matrix are tetradic matrices. The scattering matrix is causal and contains a $\theta(t'-t_1)$ factor.

In the frequency domain the Bethe Salpeter equation (A10) reads

$$\mathcal{G}^Y(\omega) = \mathcal{G}(\omega) + \mathcal{G}(\omega) \Gamma(\omega) \mathcal{G}(\omega), \quad (\text{A11})$$

where the noninteracting two-exciton Green's function \mathcal{G} is given by

$$\mathcal{G}_{mn,m'n'}(\omega) = \sum_{\xi\xi'} \psi_{\xi m} \psi_{\xi' n} \mathcal{I}_{\xi\xi'}(\omega) \psi_{\xi m'}^* \psi_{\xi' n'}^*, \quad (\text{A12})$$

and

$$\begin{aligned} \mathcal{I}_{\xi\xi'}(\omega) &\equiv \int dt I_{\xi}(t) I_{\xi'}(t) \exp(i\omega t) \\ &= \frac{i}{\omega - \Omega_{\xi} - \Omega_{\xi'} + i(\gamma_{\xi} + \gamma_{\xi'})}. \end{aligned} \quad (\text{A13})$$

By noting that $\mathcal{G}(\omega) = i(\omega - h)^{-1}$ and $\mathcal{G}^Y(\omega) = i(\omega - h - V)^{-1}$, where h and V are tetradic matrices, $\Gamma(\omega)$ can be obtained using the operator identity $\hat{A}^{-1} = \hat{B}^{-1} + \hat{B}^{-1}(\hat{B} - \hat{A})\hat{A}^{-1}$, where \hat{B} and \hat{A} are any two operators. Applying this to the Green's functions with $\hat{A} = (1/i)(\omega - h - V)$ and $\hat{B} = (1/i)(\omega - h)$ we get the Dyson equation

$$\mathcal{G}^Y(\omega) = \mathcal{G}(\omega) + \mathcal{G}(\omega)(-iV)\mathcal{G}^Y(\omega). \quad (\text{A14})$$

Comparing Eqs. (A11) and (A14) gives

$$-iV\mathcal{G}^Y(\omega) = \Gamma(\omega)\mathcal{G}(\omega). \quad (\text{A15})$$

Iterating Eq. (A14) and using Eq. (A15) finally gives

$$\begin{aligned} \Gamma(\omega) &= -iV + (-i)^2 V\mathcal{G}(\omega)V + (-i)^3 V\mathcal{G}(\omega)V\mathcal{G}(\omega)V + \dots \\ &\equiv -iV(1 + i\mathcal{G}(\omega)V)^{-1}. \end{aligned} \quad (\text{A16})$$

Thus, the calculation of the scattering matrix requires the inversion of the matrix $D = 1 + i\mathcal{G}(\omega)V$ with matrix elements,

$$D_{mn,ij}(\omega) = \delta_{mi}\delta_{nj} + i \sum_{m'n'} \mathcal{G}_{mn,m'n'}(\omega) V_{m'n',ij}. \quad (\text{A17})$$

In general this is a ($\mathcal{N}^2 \times \mathcal{N}^2$) matrix, where \mathcal{N} is the number of modes. Computing D is equivalent to finding all two-exciton states and is costly even for moderate \mathcal{N} . However, in practice the size of the scattering matrix can be reduced considerably for typical forms of the matrix V as shown in Appendix B. This is the main advantage of this method.

APPENDIX B: THE SCATTERING MATRIX FOR SPECIAL CASES

We consider the following form for the anharmonicity: $U_{mn,m'n'} = (\Delta_{m,n}/4)(\delta_{mm'}\delta_{nn'} + \delta_{mn'}\delta_{nm'})$ so that

$$\hat{H}_S = \hat{H}_0 + \sum_{mn} \frac{\Delta_{m,n}}{2} \hat{B}_m^\dagger \hat{B}_n^\dagger \hat{B}_m \hat{B}_n, \quad (\text{B1})$$

with $\Delta_{m,n} = \Delta_{n,m}$. Intramode anharmonicities, $\Delta_{m,m}$, represent the shift of the overtone ($\hat{B}_m^\dagger \hat{B}_m^\dagger |0\rangle$) energy with respect to $2\varepsilon_m$. Intermode anharmonicities, $\Delta_{m,n}$ with $m \neq n$, shift the combination band ($\hat{B}_m^\dagger \hat{B}_n^\dagger |0\rangle$) energies from $\varepsilon_m + \varepsilon_n$. Equation (A16) then gives for the scattering matrix

$$\Gamma_{mn,ij}(\omega) = -i\Delta_{m,n}(D^{-1}(\omega))_{mn,ij}. \quad (\text{B2})$$

We assume that the anharmonic potential $\Delta_{m,n}$ is nonzero only for short distances $|m-n| < l_c$, where l_c is an interaction length of the anharmonicity. The presence of $\Delta_{i,j}$ in Eq. (A17) and $\Delta_{m,n}$ in Eq. (B2) implies that $i-j$ and $m-n$ are

limited by the interaction length l_c . Therefore, the effective matrix size of the scattering matrix reduces to $\mathcal{N}l_c \times \mathcal{N}l_c$. We may then define a reduced matrix \bar{D} ,

$$\begin{aligned} \bar{D}_{ml_1,il_2}(\omega) &\equiv D_{m,m+l_1;i,i+l_2}(\omega) = \delta_{mi}\delta_{l_1l_2} \\ &+ i\mathcal{G}_{m,m+l_1;i,i+l_2}(\omega)\Delta_{i,i+l_2}, \end{aligned} \quad (\text{B3})$$

where the indices l_1 and l_2 take the values from interval $[-l_c, \dots, l_c]$. The complete scattering matrix can now be recast in terms of reduced matrix \bar{D} ,

$$\Gamma_{m,m+l_1;i,i+l_2}(\omega) \equiv \bar{\Gamma}_{m,l_1;i,l_2}(\omega) = -i\Delta_{m,m+l_1}(\bar{D}^{-1})_{ml_1,il_2}. \quad (\text{B4})$$

All other elements of Γ vanish.

As a special case we consider a local anharmonicity where we set $\Delta_{m,n} = \bar{\Delta}_m \delta_{m,n}$ (soft-core boson approximation).⁵⁷ Then

$$\bar{D}_{m0,i0}(\omega) = \delta_{mi} + i\mathcal{G}_{mm,ii}(\omega)\bar{\Delta}_i. \quad (\text{B5})$$

and the scattering matrix

$$\Gamma_{mm,nn}(\omega) = -i\bar{\Delta}_m(\bar{D}^{-1})_{m0,n0}. \quad (\text{B6})$$

Thus the excitons interact and scatter only when they occupy the same site. The interaction radius is $l_c=0$ and $\mathcal{N} \times \mathcal{N}$ matrix \bar{D} has the size as of the one-exciton basis.

For large anharmonicities each mode becomes effectively a two level system and the two excitons then cannot reside on the same site (hard-core bosons). This can be described by taking the limit $\bar{\Delta} \rightarrow \infty$ leading to^{57,90}

$$\Gamma_{mm,nn}(\omega) = -(\mathcal{G}(\omega))_{mm,nn}^{-1}. \quad (\text{B7})$$

APPENDIX C: TIME DOMAIN GREEN'S FUNCTION EXPRESSIONS FOR THE THIRD-ORDER OPTICAL RESPONSE

The NEE can be solved by order-by-order expansion of the variables in the field using the exciton Green's functions (Appendix A) where the optical field and the lower-order variables serve as the sources. The first-order variable, $B_m^{(1)}(t)$, is obtained from Eq. (4),

$$B_m^{(1)}(t) = i \int_{-\infty}^{\infty} dt' \sum_n G_{m,n}(t-t') \mathcal{E}_n(t'). \quad (\text{C1})$$

The second-order variable, $Y_{mn}^{(2)}(t)$, is then obtained from Eq. (5),

$$\begin{aligned} Y_{mn}^{(2)}(t) &= i \int_{-\infty}^{\infty} dt' \sum_{m'n'} \mathcal{G}_{mn,m'n'}^Y(t-t') (\mathcal{E}_{m'}(t') B_{n'}^{(1)}(t')) \\ &+ \mathcal{E}_{n'}(t') B_{m'}^{(1)}(t'). \end{aligned} \quad (\text{C2})$$

The third-order variable then is finally obtained from Eq. (4) in terms of the exciton Green's functions and the exciton scattering matrix

$$\begin{aligned} B_{n_4}^{(3)}(t_4) &= 2i \int_{-\infty}^{\infty} d\tau'' \int_{-\infty}^{\infty} d\tau' \int_{-\infty}^{\infty} dt_3 \int_{-\infty}^{\infty} dt_2 \int_{-\infty}^{\infty} dt_1 \\ &\sum_{n_1 n_2 n_3} \sum_{n'_1 n'_2 n'_3 n'_4} \theta(t_2 - t_1) \Gamma_{n'_4 n'_3 n'_2 n'_1}(\tau'' - \tau') \\ &\times G_{n_4 n_4}(t_4 - \tau'') G_{n'_3 n'_3}^\dagger(\tau'' - t_3) \\ &\times G_{n'_2 n'_2}(\tau' - t_2) G_{n'_1 n'_1}(\tau' - t_1) \\ &\times \mathcal{E}_{n_3}(t_3) \mathcal{E}_{n_2}(t_2) \mathcal{E}_{n_1}(t_1), \end{aligned} \quad (\text{C3})$$

where we used Eq. (A15) to change $-i \sum_{n'_2 n'_1} V_{n'_4 n'_3 n'_2 n'_1} \mathcal{G}_{n'_2 n'_1 n_2 j}^Y(\tau'' - t_2)$ into $\sum_{n'_2 n'_1} \int_{-\infty}^{\infty} d\tau' \Gamma_{n'_4 n'_3 n'_2 n'_1} \times (\tau'' - \tau') \mathcal{G}_{n'_2 n'_1 n_2 j}(\tau' - t_2)$, then we factorized $\mathcal{G}_{n'_2 n'_1 n_2 j}(\tau' - t_2) \equiv G_{n'_2 n_2}(\tau' - t_2) G_{n'_1 j}(\tau' - t_2)$ and performed a summation over index j : $\sum_j G_{n'_1 j}(\tau' - t_2) G_{j n_1}(t_2 - t_1) = G_{n'_1 n_1}(\tau' - t_1) \theta(\tau' - t_2) \theta(t_2 - t_1)$. The variables τ' and τ'' denote the times of the first and the last exciton-exciton interaction, respectively, as shown in Fig. 1(b).

We use third-order NEE variables and their Green's functions to calculate the response function. Using Eqs. (6), (1), and (C3), we obtain the response function

$$\begin{aligned} S_{\nu_4, \nu_3 \nu_2 \nu_1}^{(3)}(\mathbf{r}_4 t_4; \mathbf{r}_3 t_3, \mathbf{r}_2 t_2, \mathbf{r}_1 t_1) \\ = i \mathcal{P}_{\nu \tau} \sum_{n_4 n_3 n_2 n_1} \delta(\mathbf{r}_4 - \mathbf{r}_{n_4}) \delta(\mathbf{r}_3 - \mathbf{r}_{n_3}) \delta(\mathbf{r}_2 - \mathbf{r}_{n_2}) \delta(\mathbf{r}_1 - \mathbf{r}_{n_1}) \\ \times \mathbf{M}_{n_4 n_3 n_2 n_1}^{\nu_4 \nu_3 \nu_2 \nu_1} \sum_{n'_4 n'_3 n'_2 n'_1} \int_{-\infty}^{\infty} d\tau'' \int_{-\infty}^{\infty} d\tau' \Gamma_{n'_4 n'_3 n'_2 n'_1}(\tau'' - \tau') \\ \times G_{n_4 n_4}(t_4 - \tau'') G_{n'_3 n'_3}^\dagger(\tau'' - t_3) G_{n'_2 n'_2}(\tau' - t_2) \\ \times G_{n'_1 n_1}(\tau' - t_1) + \text{c. c.}, \end{aligned} \quad (\text{C4})$$

where $\mathbf{M}_{n_4 n_3 n_2 n_1}^{\nu_4 \nu_3 \nu_2 \nu_1} = \boldsymbol{\mu}_{n_4}^{\nu_4} \boldsymbol{\mu}_{n_3}^{\nu_3} \boldsymbol{\mu}_{n_2}^{\nu_2} \boldsymbol{\mu}_{n_1}^{\nu_1}$, c.c. denotes the complex conjugate, and $\mathcal{P}_{\nu \tau}$ denotes permutation of interaction events, which are defined by $\nu_j \mathbf{r}_j t_j$ with $j=1, 2, 3$: $(3, 2, 1) + (2, 3, 1) + (1, 2, 3)$. This makes the response function symmetric with respect to this permutation (there are only three terms since the function is inherently symmetric with respect to the permutation of 1 and 2).

The response function in the exciton basis is obtained by plugging Eq. (A4) into Eq. (C4),

$$\begin{aligned} S_{\nu_4, \nu_3 \nu_2 \nu_1}^{(3)}(\mathbf{r}_4 t_4; \mathbf{r}_3 t_3, \mathbf{r}_2 t_2, \mathbf{r}_1 t_1) \\ = i \mathcal{P}_{\nu \tau} \sum_{\xi_4 \xi_3 \xi_2 \xi_1} \mathbf{d}_{\xi_4}^{\nu_4}(\mathbf{r}_4) \mathbf{d}_{\xi_3}^{\nu_3}(\mathbf{r}_3) \mathbf{d}_{\xi_2}^{\nu_2*}(\mathbf{r}_2) \mathbf{d}_{\xi_1}^{\nu_1*}(\mathbf{r}_1) \\ \times \int_{-\infty}^{\infty} d\tau'' \int_{-\infty}^{\infty} d\tau' \Gamma_{\xi_4 \xi_3 \xi_2 \xi_1}(\tau'' - \tau') I_{\xi_4}(t_4 - \tau'') \\ \times I_{\xi_3}^*(\tau'' - t_3) I_{\xi_2}(\tau' - t_2) I_{\xi_1}(\tau' - t_1) + \text{c.c.}, \end{aligned} \quad (\text{C5})$$

where the nonlocal exciton transition dipoles are given by Eq. (15) and we have transformed the exciton scattering matrix into the exciton basis,

$$\Gamma_{\xi_4 \xi_3, \xi_2 \xi_1}(\tau) = \sum_{m_4 m_3 m_2 m_1} \psi_{\xi_4 m_4}^* \psi_{\xi_3 m_3}^* \Gamma_{m_4 m_3, m_2 m_1}(\tau) \times \psi_{\xi_2 m_2} \psi_{\xi_1 m_1}. \quad (\text{C6})$$

APPENDIX D: EIGENSTATES AND SUSCEPTIBILITIES OF PERIODIC SYSTEMS

We consider the system shown in Fig. 2. We use periodic boundary conditions to represent translational invariance and ignore edge effects. Since the system is translationally invariant, the intermode coupling $J_{\mathbf{R}m, \mathbf{R}'n} = J_{m,n}(\mathbf{R}' - \mathbf{R})$ now depends on the distance between cells $\mathbf{R}' - \mathbf{R}$ and on the sites inside each cell, m and n . Note the difference in notation with the preceding section: now each mode is represented by a pair of indices, $\mathbf{R}m$.

The one-exciton states of this system are the Bloch states. Each eigenstate ξ is represented by a pair of quantum numbers $\mathbf{q}\lambda$, where λ denotes different Davydov's subbands in the one-exciton band (there are \mathcal{M} different subbands) with momentum \mathbf{q} . The momentum \mathbf{q} assumes the values $(-\pi/a, \dots, (\pi/a) - d_q)$ including 0 in each dimension, with the step $d_q = 2\pi/L$ and $L = Na$ is the length of the system. The one-exciton Bloch states are given by

$$\psi_{\mathbf{R}m}^{(\lambda)}(\mathbf{q}) = \frac{1}{\sqrt{V}} \exp(-i\mathbf{q}\mathbf{R}) \bar{\psi}_{\lambda m}(\mathbf{q}), \quad (\text{D1})$$

where $\bar{\psi}_{\lambda m}(\mathbf{q})$ are the translationally invariant eigenstates of the cell given by

$$\sum_{m'} J_{m,m'}(\mathbf{q}) \bar{\psi}_{\lambda m'}(\mathbf{q}) = \Omega_\lambda(\mathbf{q}) \bar{\psi}_{\lambda m}(\mathbf{q}). \quad (\text{D2})$$

Here $J_{m,m'}(\mathbf{q}) = \sum_{\mathbf{r}} e^{-i\mathbf{q}\mathbf{r}} J_{m,m'}(\mathbf{r})$; the prime in the sum over m denotes the summation over sites inside one cell, while the sum over \mathbf{r} runs over cells including $\mathbf{r}=0$; λ takes values from 0 to $\mathcal{M}-1$. $J_{m,m'}(\mathbf{q})$ is a matrix of the size $\mathcal{M} \times \mathcal{M}$ with indices m and m' denoting different sites; each matrix element depends parametrically on the vector \mathbf{q} .

In the frequency domain the one-exciton Green's function is obtained from Eqs. (A6) and (A7),

$$\mathbf{G}_{\mathbf{R}m, \mathbf{R}'m'}(\omega) = \frac{1}{V} \sum_{\mathbf{q}} \sum_{\lambda} e^{i\mathbf{q}(\mathbf{R}' - \mathbf{R})} \bar{\psi}_{\lambda m}(\mathbf{q}) \bar{\psi}_{\lambda m'}^*(\mathbf{q}) I_\lambda(\mathbf{q}, \omega), \quad (\text{D3})$$

\sum' indicates the sum over different Davydov's subbands with the exciton Green's function,

$$I_\lambda(\mathbf{q}, \omega) = \frac{i}{\omega - \Omega_\lambda(\mathbf{q}) + i\gamma_\lambda(\mathbf{q})}. \quad (\text{D4})$$

Using the eigenstates and Green's functions of periodic systems in Eq. (12) we obtain the linear susceptibility,

$$\chi_{v_2, v_1}^{(1)}(-\mathbf{k}_2 - \omega_2; \mathbf{k}_1 \omega_1) = 2\pi i \delta(\omega_2 - \omega_1) \times \sum_{\mathbf{q}} \sum_{\lambda} ' \mathbf{d}_\lambda^{v_2}(\mathbf{k}_2, \mathbf{q}) \mathbf{d}_\lambda^{v_1*}(\mathbf{k}_1, \mathbf{q}) I_\lambda(\mathbf{q}, \omega_2) + \text{c.c.}', \quad (\text{D5})$$

where

$$\mathbf{d}_\lambda^v(\mathbf{k}, \mathbf{q}) = \frac{1}{\sqrt{V}} \sum_{\mathbf{R}} \sum_m ' e^{i\mathbf{k}(\mathbf{R} + \rho_m) - i\mathbf{q}\mathbf{R}} \bar{\psi}_{\lambda m}(\mathbf{q}) \boldsymbol{\mu}_m^v. \quad (\text{D6})$$

The \mathbf{R} summation (a discrete coordinate of cell) runs over the cells, \mathbf{q} is also a discrete momentum, while \mathbf{k} is a continuous vector.

The third-order susceptibility is obtained from Eq. (26) and is given by,

$$\begin{aligned} \chi_{v_4, v_3, v_2, v_1}^{(3)}(-\mathbf{k}_4, -\omega_4; \mathbf{k}_3, \omega_3, \mathbf{k}_2, \omega_2, \mathbf{k}_1, \omega_1) \\ = 2\pi i \delta(\omega_4 - \omega_3 - \omega_2 - \omega_1) \mathcal{P}_{\nu\mathbf{k}\omega} \\ \times \sum_{\mathbf{q}_4 \dots \mathbf{q}_1} \sum_{\lambda_4 \dots \lambda_1} ' \mathbf{d}_{\lambda_4}^{v_4}(\mathbf{k}_4, \mathbf{q}_4) \mathbf{d}_{\lambda_3}^{v_3}(-\mathbf{k}_3, \mathbf{q}_3) \\ \times \mathbf{d}_{\lambda_2}^{v_2*}(\mathbf{k}_2, \mathbf{q}_2) \mathbf{d}_{\lambda_1}^{v_1*}(\mathbf{k}_1, \mathbf{q}_1) \\ \times \Gamma_{\lambda_4 \lambda_3 \lambda_2 \lambda_1}(\mathbf{q}_4 \mathbf{q}_3 \mathbf{q}_2 \mathbf{q}_1, \omega_1 + \omega_2) I_{\lambda_4}(\mathbf{q}_4, \omega_4) I_{\lambda_3}^*(\mathbf{q}_3, -\omega_3) \\ \times I_{\lambda_2}(\mathbf{q}_2, \omega_2) I_{\lambda_1}(\mathbf{q}_1, \omega_1) + \text{c.c.}', \end{aligned} \quad (\text{D7})$$

where the scattering matrix is given by

$$\begin{aligned} \Gamma_{\lambda_4 \lambda_3 \lambda_2 \lambda_1}(\mathbf{q}_4, \mathbf{q}_3, \mathbf{q}_2, \mathbf{q}_1; \omega) \\ = \frac{1}{V^2} \sum_{\mathbf{R}_4 \dots \mathbf{R}_1} \exp(i\mathbf{q}_4 \mathbf{R}_4 + i\mathbf{q}_3 \mathbf{R}_3 - i\mathbf{q}_2 \mathbf{R}_2 - i\mathbf{q}_1 \mathbf{R}_1) \\ \times \sum_{m_4 \dots m_1} ' \bar{\psi}_{\lambda_4 m_4}^*(\mathbf{q}_4) \bar{\psi}_{\lambda_3 m_3}^*(\mathbf{q}_3) \Gamma_{\mathbf{R}_4 m_4 \dots \mathbf{R}_1 m_1}(\omega) \\ \times \bar{\psi}_{\lambda_2 m_2}(\mathbf{q}_2) \bar{\psi}_{\lambda_1 m_1}(\mathbf{q}_1). \end{aligned} \quad (\text{D8})$$

$\Gamma_{\mathbf{R}_4 m_4 \dots \mathbf{R}_1 m_1}(\omega)$ is the real space scattering matrix identical to Eq. (A16), where site indices n were changed into the pairs $\mathbf{R}m$. The reduced expression of the scattering matrix is given by Eq. (E7). These are the most general expressions for arbitrary oriented periodic system. The directions are given in the molecular frame. The scattering matrix can be reduced considerably as shown in Appendix E.

When the system size is much larger than the optical wavelength $|\mathbf{k}_0|L \gg 1$, \mathbf{R} and \mathbf{q} may be treated as continuous variables and the summations over \mathbf{R} and \mathbf{q} in Eqs. (D5) and (D7) can be changed into integrations. In this case the equations are considerably simplified. The linear susceptibility is

$$\begin{aligned} \chi_{v_2, v_1}^{(1)}(-\mathbf{k}_2 - \omega_2; \mathbf{k}_1 \omega_1) = (2\pi)^4 i \delta(\omega_2 - \omega_1) \delta(\mathbf{k}_2 - \mathbf{k}_1) \\ \times \sum_{\lambda} ' \mathbf{d}_\lambda^{v_2}(\mathbf{k}_2) \mathbf{d}_\lambda^{v_1*}(\mathbf{k}_2) I_\lambda(\mathbf{k}_2, \omega_2) + \text{c.c.}', \end{aligned} \quad (\text{D9})$$

where $\mathbf{d}_\lambda^v(\mathbf{k}) \equiv \mathbf{d}_\lambda^v(\mathbf{k}, \mathbf{k}) = \sqrt{V} \sum_m ' e^{i\mathbf{k}\rho_m} \bar{\psi}_{\lambda m}(\mathbf{q}) \boldsymbol{\mu}_m^v$ are the transition dipoles of infinite system between different continuous exciton bands. $I_\lambda(\mathbf{q}, \omega)$ is the exciton Green's function in the exciton basis [Eq. (D4)].

For the third-order susceptibility we obtain

$$\begin{aligned} \chi_{v_4, v_3, v_2, v_1}^{(3)}(-\mathbf{k}_4, -\omega_4; \mathbf{k}_3, \omega_3, \mathbf{k}_2, \omega_2, \mathbf{k}_1, \omega_1) = 2\pi i \delta(\omega_4 - \omega_3 - \omega_2 \\ - \omega_1) \mathcal{P}_{\nu\mathbf{k}\omega} \sum_{\lambda_4 \dots \lambda_1} ' \mathbf{d}_{\lambda_4}^{v_4}(\mathbf{k}_4) \mathbf{d}_{\lambda_3}^{v_3}(-\mathbf{k}_3) \mathbf{d}_{\lambda_2}^{v_2*}(\mathbf{k}_2) \mathbf{d}_{\lambda_1}^{v_1*}(\mathbf{k}_1) \\ \times \Gamma_{\lambda_4 \dots \lambda_1}(\mathbf{k}_4, -\mathbf{k}_3, \mathbf{k}_2, \mathbf{k}_1, \omega_1 + \omega_2) \end{aligned}$$

$$\times I_{\lambda_4}(\mathbf{k}_4, \omega_4) I_{\lambda_3}^*(-\mathbf{k}_3, -\omega_3) I_{\lambda_2}(\mathbf{k}_2, \omega_2) I_{\lambda_1}(\mathbf{k}_1, \omega_1) + \text{c.c.}' \quad (\text{D10})$$

This limit may be achieved for pure oriented semiconductors or molecular crystals at cryogenic temperatures where the exciton coherence size is larger than the wavelength. The opposite limiting case of the small systems is discussed in Sec. VI.

APPENDIX E: THE EXCITON SCATTERING MATRIX IN MOMENTUM SPACE

Computing the general scattering matrix [Eq. (D8)] is very costly for a large systems. Using a finite interaction radius l_c and periodicity we can reduce the problem size below $\mathcal{N}l_c$.

Equations (B2) and (B4) define the exciton scattering matrix by the reduced matrix \bar{D} which depends on \mathcal{G} [see Eq. (B3)]. Using the representation of Fig. 2, the two-exciton Green's function in the coordinate representation has the form $\mathcal{G}_{\mathbf{R}_m, \mathbf{R}_n; \mathbf{R}'_m, \mathbf{R}'_n}(\omega)$, where $m \dots$ are indices of sites in cells and $\mathbf{R}_m \dots$ labels different cells. The coupling and the anharmonicity matrix are now translationally invariant and can be given as $J_{m, m'}(\mathbf{r})$ and $\Delta_{m, m'}(\mathbf{r})$, respectively, where \mathbf{r} defines the distance between the cells. We are interested in the Green's function when $\mathbf{R}_n = \mathbf{R}_m + \mathbf{r}_1$ and $\mathbf{R}'_n = \mathbf{R}'_m + \mathbf{r}_2$ when \mathbf{r}_1 and \mathbf{r}_2 are within interaction radius l_c (otherwise the quartic coupling V is zero). Thus, we define the reduced Green's function $\bar{\mathcal{G}}_{\mathbf{R}_m, \mathbf{r}_1; \mathbf{R}'_m, \mathbf{r}_2}(\omega) = \mathcal{G}_{\mathbf{R}_m, (\mathbf{R}_m + \mathbf{r}_1); \mathbf{R}'_m, (\mathbf{R}'_m + \mathbf{r}_2)}$ and expand it in the basis of one-exciton eigenstates given by Eq.(D1),

$$\bar{\mathcal{G}}_{\mathbf{R}_m, \mathbf{r}_1; \mathbf{R}'_m, \mathbf{r}_2}(\omega) = \frac{1}{\mathcal{V}^2} \sum_{\mathbf{q}, \mathbf{q}'} e^{i(\mathbf{q} + \mathbf{q}')(\mathbf{R}'_m - \mathbf{R}_m) - i\mathbf{q}'(\mathbf{r}_1 - \mathbf{r}_2)} \times g_{m, n; m', n'}(\mathbf{q}, \mathbf{q}', \omega), \quad (\text{E1})$$

where the unit cell's Green's function

$$g_{m, n; m', n'}(\mathbf{q}, \mathbf{q}', \omega) = \sum_{\lambda, \lambda'} \bar{\psi}_{\lambda m}(\mathbf{q}) \bar{\psi}_{\lambda' n}(\mathbf{q}') \mathcal{I}_{\lambda, \lambda'}(\mathbf{q}, \mathbf{q}', \omega) \times \bar{\psi}_{\lambda m}^*(\mathbf{q}) \bar{\psi}_{\lambda' n}^*(\mathbf{q}') \quad (\text{E2})$$

and

$$\mathcal{I}_{\lambda, \lambda'}(\mathbf{q}, \mathbf{q}', \omega) = \frac{i}{\omega - \Omega_\lambda(\mathbf{q}) - \Omega_{\lambda'}(\mathbf{q}') + i\gamma_\lambda(\mathbf{q}) + i\gamma_{\lambda'}(\mathbf{q}')} \quad (\text{E3})$$

is a two-exciton Green's function in the frequency domain.

Taking into account the translational invariance with respect to \mathbf{R}_m and \mathbf{R}'_m we can transform the two-exciton Green's function to momentum space,

$$\bar{\mathcal{G}}_{\mathbf{r}_1, m, n; \mathbf{r}_2, m', n'}(\mathbf{q}, \omega) = \frac{1}{\mathcal{V}} \sum_{\mathbf{q}_1} e^{i(\mathbf{q} - \mathbf{q}_1)(\mathbf{r}_2 - \mathbf{r}_1)} \times g_{m, n; m', n'}(\mathbf{q}_1, \mathbf{q} - \mathbf{q}_1, \omega). \quad (\text{E4})$$

We can now write the transformed $\mathcal{M}^2 l_c \times \mathcal{M}^2 l_c$ matrix \bar{D} ,

$$\bar{D}_{\mathbf{r}_1, m, n; \mathbf{r}_2, m', n'}(\mathbf{q}, \omega) = \delta_{\mathbf{r}_1, \mathbf{r}_2} \delta_{m, m'} \delta_{n, n'} + i \bar{\mathcal{G}}_{\mathbf{r}_1, m, n; \mathbf{r}_2, m', n'}(\mathbf{q}, \omega) \Delta_{m', n'}(\mathbf{r}_2). \quad (\text{E5})$$

Note that we are using a mixed momentum and real space representation, which allows us to control the expressions using the interaction distance l_c . The transformation with respect to \mathbf{r}_1 and \mathbf{r}_2 does not simplify the expression since these coordinates are not translationally invariant in our expressions of \bar{D} . The exciton scattering matrix in this mixed representation now reads

$$\bar{\Gamma}_{\mathbf{r}_1, m, n; \mathbf{r}_2, m', n'}(\mathbf{q}, \omega) = -i \Delta_{m, n}(\mathbf{r}_1) (\bar{D}(\mathbf{q}, \omega))_{\mathbf{r}_1, m, n; \mathbf{r}_2, m', n'}^{-1}. \quad (\text{E6})$$

This expression is illustrated in Fig. 2(b). Here the initial two-exciton pair m' and n' is separated by the distance $\mathbf{r}_2 = \mathbf{R}_{n'} - \mathbf{R}_{m'}$ within interaction radius, which is established by $\Delta_{m', n'}(\mathbf{r}_2)$. The pair is scattered by the matrix $\bar{\Gamma}$ to create a new pair of excitons at m and n separated by $\mathbf{r}_1 = \mathbf{R}_n - \mathbf{R}_m$. The distance between two excitons after scattering is also within the interaction distance as required by $\Delta_{m, n}(\mathbf{r}_1)$. The distance between the two exciton pairs is not important because of translational invariance.

For the scattering matrix in the eigenstate representation we obtain

$$\Gamma_{\lambda_4 \lambda_3 \lambda_2 \lambda_1}(\mathbf{q}_4, \mathbf{q}_3, \mathbf{q}_2, \mathbf{q}_1; \omega) = \delta_{(\mathbf{q}_4 + \mathbf{q}_3), (\mathbf{q}_2 + \mathbf{q}_1)} \sum_{-l_c < \mathbf{r}' \mathbf{r}'' < l_c} \exp(i\mathbf{q}_3 \mathbf{r}'' - i\mathbf{q}_1 \mathbf{r}') \times \sum_{m_4 \dots m_1} \bar{\psi}_{\lambda_4 m_4}^*(\mathbf{q}_4) \bar{\psi}_{\lambda_3 m_3}^*(\mathbf{q}_3) \bar{\Gamma}_{\mathbf{r}'' m_4 m_3; \mathbf{r}' m_2 m_1}(\mathbf{q}_2 + \mathbf{q}_1, \omega) \times \bar{\psi}_{\lambda_2 m_2}(\mathbf{q}_2) \bar{\psi}_{\lambda_1 m_1}(\mathbf{q}_1). \quad (\text{E7})$$

The total momentum before interaction and after interaction is conserved.

The calculation of the response function [Eq. (45)] requires the scattering matrix for zero momentum. The final expressions are:

$$g_{m, n; m', n'}(\mathbf{q}, -\mathbf{q}, \omega) = \sum_{\lambda, \lambda'} \bar{\psi}_{\lambda m}(\mathbf{q}) \bar{\psi}_{\lambda' n}(-\mathbf{q}) \times \mathcal{I}_{\lambda, \lambda'}(\mathbf{q}, -\mathbf{q}, \omega) \bar{\psi}_{\lambda m}^*(\mathbf{q}) \bar{\psi}_{\lambda' n}^*(-\mathbf{q}), \quad (\text{E8})$$

$$\bar{\mathcal{G}}_{\mathbf{r}_1, m, n; \mathbf{r}_2, m', n'}(\omega) = \frac{1}{\mathcal{V}} \sum_{\mathbf{q}} e^{-i\mathbf{q}(\mathbf{r}_2 - \mathbf{r}_1)} g_{m, n; m', n'}(\mathbf{q}, -\mathbf{q}, \omega), \quad (\text{E9})$$

$$\bar{D}_{\mathbf{r}_1, m, n; \mathbf{r}_2, m', n'}(\omega) = \delta_{\mathbf{r}_1, \mathbf{r}_2} \delta_{m, m'} \delta_{n, n'} + i \bar{\mathcal{G}}_{\mathbf{r}_1, m, n; \mathbf{r}_2, m', n'}(\omega) \Delta_{m', n'}(\mathbf{r}_2), \quad (\text{E10})$$

$$\bar{\Gamma}_{\mathbf{r}_1, m, n; \mathbf{r}_2, m', n'}(\omega) = -i\Delta_{mn}(\mathbf{r}_1)(\bar{D}(\omega))_{\mathbf{r}_1, m, n; \mathbf{r}_2, m', n'}^{-1}, \quad (\text{E11})$$

and the Green's function of the unit cell were given by Eq. (E2). The scattering matrix of the eigenstates is

$$\Gamma_{\lambda_4 \lambda_3 \lambda_2 \lambda_1}(\omega) = \sum_{-l_c < \mathbf{r}' \mathbf{r}'' < l_c} \sum_{m_4 \dots m_1} \bar{\psi}_{\lambda_4 m_4} \bar{\psi}_{\lambda_3 m_3} \bar{\Gamma}_{\mathbf{r}' m_4 m_3; \mathbf{r}'' m_2 m_1}(\omega) \times \bar{\psi}_{\lambda_2 m_2} \bar{\psi}_{\lambda_1 m_1}. \quad (\text{E12})$$

The matrix sizes are $\mathcal{M}^2(2l_c+1) \times \mathcal{M}^2(2l_c+1)$, the same size as for the inversion problem. These are significantly reduced compared to nonperiodic systems.

APPENDIX F: TIME-DOMAIN OPTICAL RESPONSE FUNCTIONS

Time-domain expressions are useful for experiments performed with ultrafast, well separated, optical pulses. The sequence of interactions can then be defined and different techniques can be determined by their time ordering.⁴⁰ The time ordered optical response is defined by

$$\mathbf{P}_{\nu_4}^{(3)}(\mathbf{r}_4, t_4) = \sum_{\nu_3 \nu_2 \nu_1} \int d\mathbf{r}_3 \int d\mathbf{r}_2 \int d\mathbf{r}_1 \int_{-\infty}^{t_4} dt_3 \int_{-\infty}^{t_3} dt_2 \int_{-\infty}^{t_2} dt_1 \mathcal{S}_{\nu_4, \nu_3 \nu_2 \nu_1}^{(3)}(\mathbf{r}_4 t_4; \mathbf{r}_3 t_3, \mathbf{r}_2 t_2, \mathbf{r}_1 t_1) \mathbf{E}_{\nu_3}(\mathbf{r}_3, t_3) \mathbf{E}_{\nu_2}(\mathbf{r}_2, t_2) \mathbf{E}_{\nu_1}(\mathbf{r}_1, t_1), \quad (\text{F1})$$

where t_1 now stands for the first interaction, t_2 for the second, and t_3 for the third in chronological order.

Equation. (C4) cannot be used directly since the time arguments have to be rearranged in chronological order. To that end we separate the expression into three terms:

$$\mathcal{S}_{\nu_4, \nu_3 \nu_2 \nu_1}^{(3)}(\mathbf{r}_4 t_4, \dots, \mathbf{r}_1 t_1) = \mathcal{S}_{\nu_4, \nu_3 \nu_2 \nu_1}^{\mathbf{k}_I}(\mathbf{r}_4 t_4, \dots, \mathbf{r}_1 t_1) + \mathcal{S}_{\nu_4, \nu_3 \nu_2 \nu_1}^{\mathbf{k}_{II}}(\mathbf{r}_4 t_4, \dots, \mathbf{r}_1 t_1) + \mathcal{S}_{\nu_4, \nu_3 \nu_2 \nu_1}^{\mathbf{k}_{III}}(\mathbf{r}_4 t_4, \dots, \mathbf{r}_1 t_1) + \text{c.c.}, \quad (\text{F2})$$

where

$$\mathcal{S}_{\nu_4, \nu_3 \nu_2 \nu_1}^{\mathbf{k}_I}(\mathbf{r}_4 t_4, \dots, \mathbf{r}_1 t_1) = 2i \sum_{n_4 \dots n_1} \langle \delta(\mathbf{r}_4 - \mathbf{r}_{n_4}) \dots \delta(\mathbf{r}_1 - \mathbf{r}_{n_1}) \rangle \times \mathbf{M}_{n_4 \dots n_1}^{\nu_4 \dots \nu_1} \mathcal{J}_{n_4 n_1 n_3 n_2}(t_4, t_4, t_4), \quad (\text{F3})$$

$$\mathcal{S}_{\nu_4, \nu_3 \nu_2 \nu_1}^{\mathbf{k}_{II}}(\mathbf{r}_4 t_4, \dots, \mathbf{r}_1 t_1) = 2i \sum_{n_4 \dots n_1} \langle \delta(\mathbf{r}_4 - \mathbf{r}_{n_4}) \dots \delta(\mathbf{r}_1 - \mathbf{r}_{n_1}) \rangle \times \mathbf{M}_{n_4 \dots n_1}^{\nu_4 \dots \nu_1} \mathcal{J}_{n_4 n_2 n_3 n_1}(t_4, t_4, t_4), \quad (\text{F4})$$

$$\mathcal{S}_{\nu_4, \nu_3 \nu_2 \nu_1}^{\mathbf{k}_{III}}(\mathbf{r}_4 t_4, \dots, \mathbf{r}_1 t_1) = 2i \sum_{n_4 \dots n_1} \langle \delta(\mathbf{r}_4 - \mathbf{r}_{n_4}) \dots \delta(\mathbf{r}_1 - \mathbf{r}_{n_1}) \rangle \times \mathbf{M}_{n_4 \dots n_1}^{\nu_4 \dots \nu_1} \mathcal{J}_{n_4 n_3 n_2 n_1}(t_4, t_4, t_4), \quad (\text{F5})$$

and we have defined an auxiliary function

$$\mathcal{J}_{n_4 n_3 n_2 n_1}(\tau_3, \tau_2, \tau_1) = \sum_{n'_4 n'_3 n'_2 n'_1} \int_0^{\tau_2} d\tau''_s \int_0^{\tau''_s} d\tau'_s \Gamma_{n'_4 n'_3 n'_2 n'_1}(\tau''_s - \tau'_s) \times G_{n_4 n'_4}(\tau'_s) G_{n'_3 n_3}^{\dagger}(\tau_3 - \tau'_s) \times G_{n'_2 n_2}(\tau_2 - \tau''_s) G_{n'_1 n_1}(\tau_1 - \tau''_s). \quad (\text{F6})$$

Here $t_{ij} = t_i - t_j$ is the time delay between two consecutive interactions. τ'_s and τ''_s are the delay times between exciton scattering events and the polarization measurement: $\tau'_s = t_4 - \tau''_s$, $\tau''_s = t_4 - \tau'_s$ as shown in Fig. 1(b). Since the time variables can be rearranged as t_{43} , $t_{42} = t_{43} + t_{32}$, $t_{41} = t_{43} + t_{32} + t_{21}$, each response function now depends on three time delays between different interactions: t_{43} , t_{32} , and t_{21} .

The time intervals of Eqs. (F3)–(F5) and their relation to the actual interaction times are shown in Fig. 1(b). The signal can be interpreted similarly to the frequency domain susceptibility: there are three interactions with the optical fields at times $t_1 \leq t_2 \leq t_3$ which generate three quasiparticles represented by one-exciton Green's functions $G_{n'_1 n_1}$, $G_{n'_2 n_2}$, and $G_{n'_3 n_3}^{\dagger}$ (two having positive oscillation frequency and one having negative). These quasiparticles evolve in time and two of them with the same phase are scattered by $\Gamma_{n'_4 n'_3 n'_2 n'_1}$ shifting the particles to the positions n'_3 and n'_2 . The scattering is such that one of the two new excitons corresponds to the exciton generated by the field. The other exciton generates the optical response.

The time evolution is followed explicitly and the resonant terms can be selected according to wave vectors of optical fields and time ordering of the interaction. The three different time evolutions for the time ordered response functions are showed in Fig. 10.

The dependence on the wave vector of the optical field can be obtained by applying spatial Fourier transform to the response function. The expressions are considerably simplified in eigenstate basis where we get

$$\mathcal{J}_{\xi_4 \xi_3 \xi_2 \xi_1}(\tau_3, \tau_2, \tau_1) = \int_0^{\tau_2} d\tau''_s \int_0^{\tau''_s} d\tau'_s \Gamma_{\xi_4 \xi_3 \xi_2 \xi_1}(\tau''_s - \tau'_s) \times I_{\xi_4}(\tau'_s) I_{\xi_3}^*(\tau_3 - \tau'_s) I_{\xi_2}(\tau_2 - \tau''_s) \times I_{\xi_1}(\tau_1 - \tau''_s) \quad (\text{F7})$$

and

$$\mathcal{S}_{\nu_4, \nu_3 \nu_2 \nu_1}^{\mathbf{k}_I}(\mathbf{k}_4 t_4, \dots, \mathbf{k}_1 t_1) = 2i \sum_{\xi_4 \dots \xi_1} \langle \mathbf{d}_{\xi_4}^{\nu_4}(\mathbf{k}_4) \mathbf{d}_{\xi_3}^{\nu_3*}(-\mathbf{k}_3) \mathbf{d}_{\xi_2}^{\nu_2*}(-\mathbf{k}_2) \mathbf{d}_{\xi_1}^{\nu_1}(\mathbf{k}_1) \rangle \times \mathcal{J}_{\xi_4 \xi_3 \xi_2 \xi_1}(t_4, t_4, t_4), \quad (\text{F8})$$

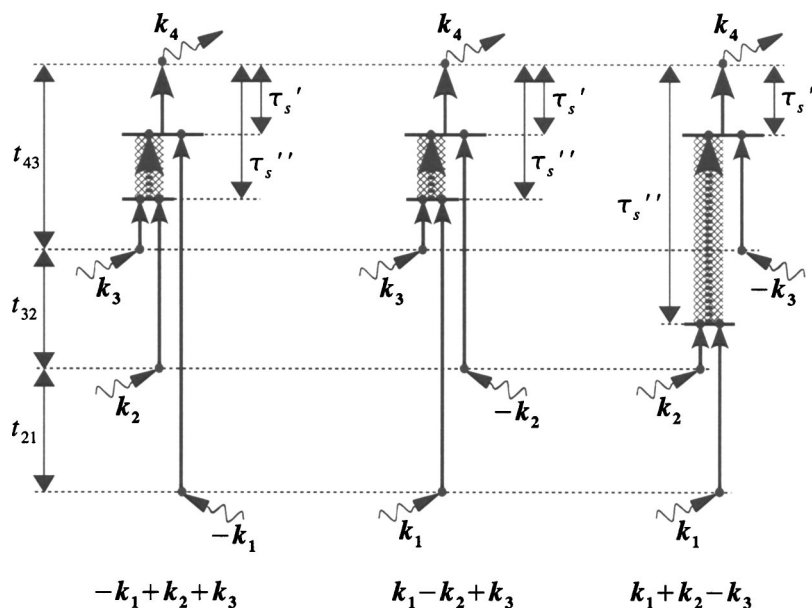


FIG. 10. (Color online) The Green's functions and the scattering matrix representing three contributions to the time-domain third-order response (adopted from Ref. 64).

$$\begin{aligned}
 & S_{\nu_4, \dots, \nu_1}^{\mathbf{k}_{II}}(\mathbf{k}_4 t_4, \dots, \mathbf{k}_1 t_1) \\
 &= 2i \sum_{\xi_4 \dots \xi_1} \langle \mathbf{d}_{\xi_4}^{\nu_4}(\mathbf{k}_4) \mathbf{d}_{\xi_3}^{\nu_3*}(-\mathbf{k}_3) \mathbf{d}_{\xi_2}^{\nu_2}(\mathbf{k}_2) \mathbf{d}_{\xi_1}^{\nu_1*}(-\mathbf{k}_1) \rangle \\
 & \quad \times \mathcal{J}_{\xi_4 \xi_2 \xi_3 \xi_1}(t_{42}, t_{43}, t_{41}), \quad (\text{F9})
 \end{aligned}$$

$$\begin{aligned}
 & S_{\nu_4, \dots, \nu_1}^{\mathbf{k}_{III}}(\mathbf{k}_4 t_4, \dots, \mathbf{k}_1 t_1) \\
 &= 2i \sum_{\xi_4 \dots \xi_1} \langle \mathbf{d}_{\xi_4}^{\nu_4}(\mathbf{k}_4) \mathbf{d}_{\xi_3}^{\nu_3}(\mathbf{k}_3) \mathbf{d}_{\xi_2}^{\nu_2*}(-\mathbf{k}_2) \mathbf{d}_{\xi_1}^{\nu_1*}(-\mathbf{k}_1) \rangle \\
 & \quad \times \mathcal{J}_{\xi_4 \xi_3 \xi_2 \xi_1}(t_{43}, t_{42}, t_{41}), \quad (\text{F10})
 \end{aligned}$$

with $\mathbf{k}_4 = -\mathbf{k}_3 - \mathbf{k}_2 - \mathbf{k}_1$ which reduces \mathcal{J} from fourfold summation to none. The dependence on the wave vectors is also expressed clearly. The rotational averages of these quantities were given in Sec. V.

Three possible techniques, $\mathbf{k}_I = -\mathbf{k}_1 + \mathbf{k}_2 + \mathbf{k}_3$, $\mathbf{k}_{II} = \mathbf{k}_1 - \mathbf{k}_2 + \mathbf{k}_3$, $\mathbf{k}_{III} = \mathbf{k}_1 + \mathbf{k}_2 - \mathbf{k}_3$, are now defined by the response functions $S^{\mathbf{k}_I}$, $S^{\mathbf{k}_{II}}$, and $S^{\mathbf{k}_{III}}$, respectively. The parameters of the response functions are the three time delays t_{43} , t_{32} , t_{21} . Consider the techniques $\mathbf{k}_I = -\mathbf{k}_1 + \mathbf{k}_2 + \mathbf{k}_3$ and $\mathbf{k}_{III} = \mathbf{k}_1 + \mathbf{k}_2 - \mathbf{k}_3$. For \mathbf{k}_I we set the second time delay $t_{32} = 0$ and perform the Fourier transforms with respect to the first and third time delays: $t_{21} \rightarrow \omega_1$ and $t_{43} \rightarrow \omega_3$. For \mathbf{k}_{III} we set the first time delay $t_{21} = 0$ and perform the Fourier transforms with respect to the second and third time delays: $t_{32} \rightarrow \omega_2$ and $t_{43} \rightarrow \omega_3$. The signals become also a function of the directions of optical wave vectors in first-order approach we are using. Expression especially useful for numerical simulations for the 2D signal in the \mathbf{k}_I technique ($\mathbf{k}_4 = -\mathbf{k}_I$) is

$$\begin{aligned}
 & W_{\nu_4, \nu_3, \nu_2, \nu_1}(\mathbf{k}_4, \mathbf{k}_3, \mathbf{k}_2, \mathbf{k}_1; \omega_1, \omega_3) \\
 &= 2i \sum_{\xi_4 \dots \xi_1} \langle \mathbf{d}_{\xi_4}^{\nu_4}(\mathbf{k}_4) \mathbf{d}_{\xi_3}^{\nu_3*}(-\mathbf{k}_3) \mathbf{d}_{\xi_2}^{\nu_2*}(-\mathbf{k}_2) \mathbf{d}_{\xi_1}^{\nu_1}(-\mathbf{k}_1) \rangle \\
 & \quad \times I_{\xi_1}^*(-\omega_1) I_{\xi_4}(\omega_3) \\
 & \quad \times \int_{-\infty}^{\infty} \frac{d\omega'}{2\pi} \Gamma_{\xi_4 \xi_1, \xi_3 \xi_2}(\omega') \mathcal{I}_{\xi_3 \xi_2}(\omega') I_{\xi_1}^*(\omega' - \omega_3)
 \end{aligned}$$

and in \mathbf{k}_{III} technique ($\mathbf{k}_4 = -\mathbf{k}_{III}$)

$$\begin{aligned}
 & W_{\nu_4, \nu_3, \nu_2, \nu_1}(\mathbf{k}_4, \mathbf{k}_3, \mathbf{k}_2, \mathbf{k}_1; \omega_2, \omega_3) \\
 &= 2i \sum_{\xi_4 \dots \xi_1} \langle \mathbf{d}_{\xi_4}^{\nu_4}(\mathbf{k}_4) \mathbf{d}_{\xi_3}^{\nu_3}(-\mathbf{k}_3) \mathbf{d}_{\xi_2}^{\nu_2*}(-\mathbf{k}_2) \mathbf{d}_{\xi_1}^{\nu_1*}(-\mathbf{k}_1) \rangle \\
 & \quad \times I_{\xi_4}(\omega_3) \int_{-\infty}^{\infty} \frac{d\omega'}{2\pi} \Gamma_{\xi_4 \xi_3, \xi_2 \xi_1}(\omega') \mathcal{I}_{\xi_2 \xi_1}(\omega') \\
 & \quad \times I_{\xi_3}^*(\omega' - \omega_3) \theta(\omega_2 - \omega').
 \end{aligned}$$

The function $\theta(\omega) = i(\omega + i\gamma')^{-1}$ is taken in the limit $\gamma_\xi \gg \gamma'$ > 0 .

- ¹L. D. Barron, *Molecular Light Scattering and Optical Activity*, 2nd ed. (Cambridge University Press, Cambridge, 2004).
- ²*Chirality Physical Chemistry*, edited by J. M. Hicks (Oxford University Press, Oxford, 2002).
- ³A. Moscowitz, *Adv. Chem. Phys.* **4**, 67 (1962).
- ⁴I. Tinoco, *Adv. Chem. Phys.* **4**, 113 (1962).
- ⁵*Circular Dichroism. Principles and Applications*, 2nd ed., edited by N. Berova, R. W. Woody, and K. Nakanishi (Wiley, New York, 2000).
- ⁶N. J. Greenfield, *Anal. Biochem.* **235**, 1 (1996).
- ⁷N. Sreerama and R. W. Woody, *Anal. Biochem.* **287**, 252 (2000).
- ⁸N. Sreerama and R. W. Woody, *Protein Sci.* **12**, 384 (2003).
- ⁹N. J. Greenfield and G. D. Fasman, *Biochemistry* **8**, 4108 (1969).
- ¹⁰J. D. Hirst, *J. Chem. Phys.* **109**, 782 (1998).
- ¹¹D. H. Chin, R. W. Woody, C. A. Rohl, and R. L. Baldwin, *Proc. Natl. Acad. Sci. U.S.A.* **99**, 15416 (2002).
- ¹²R. W. Woody, *J. Chem. Phys.* **49**, 4797 (1968).
- ¹³P. M. Bayley, E. B. Nielsen, and J. A. Shellman, *J. Phys. Chem.* **73**, 228 (1969).
- ¹⁴K. A. Bode and J. Applequist, *J. Phys. Chem.* **100**, 17825 (1996).
- ¹⁵K. A. Bode and J. Applequist, *Macromolecules* **30**, 2144 (1997).
- ¹⁶G. Kurapat, P. Kruger, A. Wolimer, J. Fleischhauer, B. Kramer, A. Zobel, A. Koslowski, H. Botterweck, and R. W. Woody, *Biopolymers* **41**, 267 (1997).
- ¹⁷P. J. Stephens and M. A. Lowe, *Annu. Rev. Phys. Chem.* **36**, 213 (1985).
- ¹⁸L. A. Nafie, *Annu. Rev. Phys. Chem.* **48**, 357 (1997).
- ¹⁹F. Eker, X. Cao, L. A. Nafie, Q. Huang, and R. Schweitzer-Stenner, *J. Phys. Chem. B* **107**, 358 (2003).
- ²⁰L. Hecht and L. D. Barron, *Raman Optical Activity in Modern Techniques in Raman Spectroscopy*, edited by J. J. Laserna, p. 265 (Wiley, New York, 1996); L. D. Barron, L. Hecht, I. H. McColl, E. W. Blanch, *Mol. Phys.* **102**, 731 (2004).
- ²¹L. D. Barron, E. W. Blanch, I. H. McColl, C. D. Syme, L. Hecht, and K.

- Nielsen, *Spectroscopy* (Amsterdam), **17**, 101 (2003).
- ²²I. H. McColl, E. W. Blanch, A. C. Gill, A. G. O. Rhie, L. Ritchie, M. A. Hecht, K. Nielsen, and L. D. Barron, *J. Am. Chem. Soc.* **125**, 10019 (2003).
- ²³B. B. Lal and L. A. Nafie, *Biopolymers* **21**, 2161 (1982).
- ²⁴S. C. Yasui, T. A. Keiderling, G. M. Bonora, and C. Toniolo, *Biopolymers* **25**, 79 (1986).
- ²⁵P. Bour, J. Kubelka, and T. A. Keiderling, *Biopolymers* **53**, 380 (2000).
- ²⁶J. Kubelka, R. A. Gangani, D. Silva, and T. A. Keiderling, *J. Am. Chem. Soc.* **124**, 5325 (2002).
- ²⁷J. Hilario, J. Kubelka, and T. A. Keiderling, *J. Am. Chem. Soc.* **125**, 7562 (2003).
- ²⁸J. Hilario, J. Kubelka, F. A. Syud, T. A. Gellman, and S. H. Keiderling, *Biopolymers* **67**, 233 (2002).
- ²⁹T. B. Freedman and L. A. Nafie, in *Modern Nonlinear Optics; part 3*, edited by M. Evans and S. Kielich (Wiley, New York 1994), p. 207.
- ³⁰J. R. Cheesema, M. J. Frisch, F. J. Devlin, and P. J. Stephens, *Chem. Phys. Lett.* **252**, 211 (1996).
- ³¹P. J. Stephens, C. S. Ashvar, F. J. Devlin, J. R. Cheesema, and M. J. Frisch, *Mol. Phys.* **89**, 579 (1996).
- ³²P. J. Stephens and F. J. Devlin, *Chirality* **12**, 172 (2000).
- ³³P. Bour, J. Sopkova, L. Bednarova, P. Malon, and T. A. Keiderling, *J. Comput. Chem.* **18**, 646 (1997).
- ³⁴J. H. Choi and M. Cho, *J. Chem. Phys.* **120**, 4383 (2004).
- ³⁵N. Sreerama, S. Y. Venyaminov, and R. W. Woody, *Protein Sci.* **8**, 370 (1999).
- ³⁶N. Sreerama, R. W. Venyaminov, and S. Y. Woody, *Anal. Biochem.* **287**, 243 (2000).
- ³⁷V. Baumruk, P. Pancoska, and T. A. Keiderling, *J. Mol. Biol.* **259**, 774 (1996).
- ³⁸P. L. Polavarapu and Z. Deng, *Faraday Discuss.* **99**, 151 (1994).
- ³⁹A. F. Bell, L. Hecht, and L. D. Barron, *J. Am. Chem. Soc.* **120**, 5820 (1998).
- ⁴⁰S. Mukamel, *Principles of Nonlinear Optical Spectroscopy* (Oxford University Press, New York, 1995).
- ⁴¹O. J. G. Somsen, R. van Grondelle, and H. van Amerogen, *Biophys. J.* **71**, 1934 (1996).
- ⁴²H. van Amerogen, L. Valkunas, and R. van Grondelle, *Photosynthetic Excitons* (World Scientific, Singapore, 2000).
- ⁴³C. Didraga, J. A. Klugkist, and J. Knoester, *J. Phys. Chem. B* **106**, 11474 (2002).
- ⁴⁴T. Wagersreiter and S. Mukamel, *J. Chem. Phys.* **105**, 7995 (1996).
- ⁴⁵M. Cho, G. R. Fleming, and S. Mukamel, *J. Chem. Phys.* **98**, 5314 (1993).
- ⁴⁶M. Cho, *J. Chem. Phys.* **119**, 7003 (2003).
- ⁴⁷S. Mukamel and D. Abramavicius, *Chem. Rev. (Washington, D.C.)* **104**, 2073 (2004).
- ⁴⁸D. L. Andrews and T. Thirunamachandran, *J. Chem. Phys.* **67**, 5026 (1977).
- ⁴⁹R. M. Hochstrasser, *Chem. Phys.* **266**, 273 (2001).
- ⁵⁰M. T. Zanni, N.-H. Ge, Y. S. Kim, and R. M. Hochstrasser, *Proc. Natl. Acad. Sci. U.S.A.* **98**, 11265 (2001).
- ⁵¹O. Golonzka and A. Tokmakoff, *J. Chem. Phys.* **115**, 297 (2001).
- ⁵²E. C. Fulmer, P. Mukherjee, A. T. Krummel, and M. T. Zanni, *J. Chem. Phys.* **120**, 8067 (2004).
- ⁵³J. Dreyer, A. M. Moran, and S. Mukamel, *Bull. Korean Chem. Soc.* **24**, 1091 (2003).
- ⁵⁴F. C. Spano and S. Mukamel, *Phys. Rev. A* **40**, 5783 (1989).
- ⁵⁵F. C. Spano and S. Mukamel, *Phys. Rev. Lett.* **66**, 1197 (1991).
- ⁵⁶F. C. Spano and S. Mukamel, *J. Chem. Phys.* **95**, 7526 (1991).
- ⁵⁷J. A. Leegwater and S. Mukamel, *Phys. Rev. A* **46**, 452 (1992).
- ⁵⁸T. Meier, V. Chernyak, and S. Mukamel, *J. Phys. Chem. B* **101**, 7332 (1997).
- ⁵⁹M. Bernarz and J. Knoester, *J. Phys. Chem. B* **105**, 12913 (2001).
- ⁶⁰D. Abramavicius and S. Mukamel, *J. Phys. Chem. B* **108**, 10295 (2004).
- ⁶¹O. Kuhn, V. Chernyak, and S. Mukamel, *J. Chem. Phys.* **105**, 8586 (1996).
- ⁶²A. Piryatinski, V. Chernyak, and S. Mukamel, *Chem. Phys.* **266**, 311 (2001).
- ⁶³C. Scheurer, A. Piryatinski, and S. Mukamel, *J. Am. Chem. Soc.* **123**, 3114 (2001).
- ⁶⁴V. Chernyak, W. M. Zhang, and S. Mukamel, *J. Chem. Phys.* **109**, 9587 (1998).
- ⁶⁵K. L. C. Hunt, *J. Chem. Phys.* **78**, 6149 (1983).
- ⁶⁶K. L. C. Hunt, *J. Chem. Phys.* **116**, 5440 (2002).
- ⁶⁷Y. R. Shen, *The Principles of Nonlinear Optics* (Wiley, New York, 1984).
- ⁶⁸W. Domcke and G. Stock, *Adv. Chem. Phys.* **100**, 1 (1997).
- ⁶⁹D. P. Craig and T. Thirunamachandran, *Molecular Quantum Electrodynamics. An Introduction to Radiation Molecule Interactions* (Dover, Mineola, NY, 1998).
- ⁷⁰D. Abramavicius, W. Zhuang, and S. Mukamel, *J. Phys. Chem. B* **108**, 18034 (2004).
- ⁷¹Z. Chi, X. G. Chen, S. W. Holtz, and S. A. Asher, *Biochemistry* **37**, 2854 (1998).
- ⁷²S. Woutersen and P. Hamm, *J. Chem. Phys.* **115**, 7737 (2001).
- ⁷³C. Fang, J. Wang, Y. S. Kim, A. K. Charnley, W. Barber-Armstrong, A. B. Smith III, S. M. Decatur, and R. M. Hochstrasser, *J. Phys. Chem. B* **108**, 10415 (2004).
- ⁷⁴H. Torii and M. Tasumi, *J. Chem. Phys.* **96**, 3379 (1992).
- ⁷⁵D. Marsh, M. Müller, and F.-J. Schmitt, *Biophys. J.* **78**, 2499 (2000).
- ⁷⁶S. Ham, S. Hahn, C. Lee, T.-K. Kim, K. Kwak, and M. Cho, *J. Phys. Chem. B* **108**, 9333 (2004).
- ⁷⁷A. Piryatinski, S. A. Asher, and S. Mukamel, *J. Phys. Chem. A* **106**, 3524 (2002).
- ⁷⁸T. Kobayashi, *J-Aggregates* (World Scientific, Singapore, 1996).
- ⁷⁹D. L. Andrews, P. Allcock, and A. A. Demidov, *Chem. Phys.* **190**, 1 (1995).
- ⁸⁰P. A. D. L. Andrews, *Optical Harmonics in Molecular Systems* (Wiley-VCH, New York, 2002).
- ⁸¹*Nonlinear Optical Properties of Organic Molecules and Crystals*, edited by D. S. Chemla and J. Zyss (Academic, New York, 1987), Vols. 1 and 2.
- ⁸²B. Dick, G. Stegeman, R. Twieg, and J. Zyss, *Chem. Phys.*, Special issue, *Molecular Nonlinear Optics: Materials, Phenomena and Devices*, **245** (1999).
- ⁸³B. Champagne, P. Fischer, and A. D. Buckingham, *Chem. Phys. Lett.* **331**, 83 (2000).
- ⁸⁴P. Fischer, A. D. Buckingham, and A. C. Albrecht, *Phys. Rev. A* **64**, 053816 (2001).
- ⁸⁵P. Fisher, F. W. Wise, and A. C. Albrecht, *J. Phys. Chem. A* **107**, 8232 (2003).
- ⁸⁶M. A. Belkin, S. H. Han, X. Wei, and Y. R. Shen, *Phys. Rev. Lett.* **87**, 113001 (2001).
- ⁸⁷P. Fischer, K. Beckwitt, F. W. Wise, and A. C. Albrecht, *Chem. Phys. Lett.* **352**, 463 (2002).
- ⁸⁸K. Kwac and M. Cho, *J. Chem. Phys.* **119**, 2247 (2003).
- ⁸⁹A. M. Moran, S.-M. Park, J. Dreyer, and S. Mukamel, *J. Chem. Phys.* **118**, 3651 (2003).
- ⁹⁰G. Juzeliunas and J. Knoester, *J. Chem. Phys.* **112**, 2325 (2000).